This is a preprint, the final version is subject to change, of the American Mineralogist (MSA)
Cite as Authors (Year) Title. American Mineralogist, in press.
DOI: http://dx.doi.org/10.2138/am-2018-6143

Revision 2

Chlorine incorporation into amphibole and biotite in high-grade iron-formations: interplay between crystallography and metamorphic fluids

DARRELL J. HENRY[1] AND NICHOLAS M. DAIGLE[1]

[1]Department of Geology and Geophysics, Louisiana State University, Baton Rouge, LA, USA.

ABSTRACT

Minor amounts of markedly Cl-rich amphibole and biotite are found in the Archean (2.8-2.9 Ga) iron-formation lithologies from the eastern Beartooth Mountains, Montana, USA. These rocks are typified by mineral assemblages of quartz + magnetite + orthopyroxene + garnet ± clinopyroxene ± plagioclase having equilibrated during granulite facies conditions of ~775–800°C and 6–8 kbar. The metamorphic Cl-rich amphibole and biotite are prograde and occur as inclusions in orthopyroxene and garnet as well as in the matrix. The high-grade Fe-rich amphiboles (mostly Cl-rich potassic-hastingsite and magnesio-ferri-hornblende) and biotites contain concentrations of Cl reaching up to 2.9 wt% and 3.4 wt%, respectively. Biotites contain up to 10.5 wt% BaO and 6.9 wt% TiO_2. Substitution of Cl into amphibole and biotite is more likely where Cl-bearing anion sites are enlarged. In amphibole threshold values of the X_{Fe2+}, ^{A}K and ^{T}Al appear to be a precondition before significant amounts of Cl are incorporated into the structure. In biotite, in addition to X_{Fe2+}, substitution of ^{T}Al also is positively correlated with Cl. The high Cl content in the minerals is suggestive of a coexisting high salinity aqueous fluid. Based on calculations using mineral chemistry, estimations of the aqueous fluid composition indicate a Cl-rich aqueous fluid (~25 wt% NaCl) with f_{H2O}/f_{HCl} ratios of ~0.68-0.82. There is evidence for brine-CO_2 immiscibility during peak metamorphism. In amphibole once the threshold values for significant Cl incorporation are attained, the Fe^{2+}-Mg partitioning of the amphibole and the coexisting mafic silicates changes such that the amphibole more favorably

Always consult and cite the final, published document. See http:/www.minsocam.org or GeoscienceWorld

partitions Fe^{2+}. A feedback mechanism can be generated such that the more Cl available from a fluid the more Fe^{2+}-rich the amphibole can become, and this produces a crystal structure that can accommodate more Cl which makes this amphibole more favorable for Fe^{2+} incorporation, and the cycle continues until Cl saturation in the crystal structures is reached or aqueous Cl^- is fully equilibrated with the amphibole.

Keywords: chlorine; iron-formation; amphibole; biotite; Archean

INTRODUCTION

Chlorine (Cl) enrichment in amphibole and biotite has been observed in a variety of terrestrial and extraterrestrial geological environments. Terrestrial Cl-rich amphibole and biotite are typically found in subsolidus metamorphic/metasomatic petrologic settings over variable pressure and temperature conditions. Fluid systems associated with Cl-rich amphibole and biotite ranges from dynamic systems in which saline aqueous fluids flux through the rocks to more static environments in which aqueous fluids become more saline through loss of H_2O from the system or through CO_2-brine immiscibility (e.g. Manning and Aranovich 2014). Terrestrial petrologic settings include skarns, calcareous metasediments, felsic and mafic granulite-facies rocks, amphibolites, ore deposits (e.g. Au, Pb-Zn, and Ni-Cu), ductile shear zones in mafic rocks, mafic eclogites, igneous rocks with subsolidus hydrothermal interactions and granulite-facies iron-formations (e.g. Krutov and Vinogradova 1966; Jacobsen 1975; Dick and Robinson 1979; Kamineni et al. 1982; Vanko 1986; Suwa et al. 1987; Henry 1988; Castelli 1988; Mora and Valley 1989; Morrison 1991; Tracy 1991; Enami et al. 1992; Oen and Lustenhouwer 1992; Pan and Fleet; Jiang et al. 1994; Kullerud 1995, 1996, 2000; Léger et al. 1996; Markl and Piazolo 1998; Kullerud and Erambert 1999, McCormick and McDonald 1999; Xiao et al. 2005; Liu et al., 2009; Uher et al., 2014; Bonin and Tatu 2016). Cl concentration levels of terrestrial minerals can

Always consult and cite the final, published document. See http:/www.minsocam.org or GeoscienceWorld

be high with amphibole containing up to 6.51 wt% Cl and biotite containing up to 7.45 wt% Cl (Jacobsen 1975; Uher et al. 2014, respectively). The extraterrestrial occurrence of amphibole with very high Cl (up to 7.0 wt%) has been documented in the nakhlite class of martian meteorites in which extreme Cl enrichment is found in amphibole associated with a late-forming melt inclusions and melt-exsolved saline aqueous fluids (e.g. Giesting and Filiberto 2016). Variations in the Cl contents of amphibole and biotite in these settings are considered to be a function of temperature, pressure, crystallographic factors, and fluid composition (e.g. Volfinger et al. 1985; Henry 1988; Morrison 1991; Zhu and Sverjensky 1991, 1992; Manning and Aranovich 2014; Daigle 2015). Of particular interest for this paper is that under high-grade metamorphic conditions, amphibole and biotite tend to either break down to anhydrous minerals (e.g. pyroxene, garnet, and feldspar), deprotonate the hydroxyl-anion to an oxy-anion and/or incorporate halogens such as Cl^- and F^- into the *O*(3) and *O*(4) anion sites of amphibole and biotite, respectively. Deprotonation of the hydroxyl anion or fluorine incorporation effectively extends the thermal stability of these typically "hydrous" minerals (e.g. Tsunogae et al. 2003; Popp et al. 2006). For magnesian or intermediate Fe^{2+}-Mg mineral compositions the smaller anions, OH^- (1.38Å) and F^- (1.31Å), readily fit in the *O*(3) and *O*(4) anion sites with bonding occurring only to local cation sites, but the larger Cl^- (1.81Å) does not fit as readily into the anion sites of these minerals if they have magnesian or intermediate Fe^{2+}-Mg compositions, and Cl is generally found in trace-to-minor amounts (Volfinger et al. 1985; Hawthorne and Oberti 2007). However, Cl is more commonly present in significant quantities in K-bearing, Fe-rich amphibole and biotite, typically with larger unit cell volumes, and from environments associated with highly saline aqueous fluids (Volfinger et al. 1985; Henry 1988; Zhu et al., 1994). As such, high-grade iron-formations should be optimal lithologic environments for examining the manner in which Cl is accommodated into

Always consult and cite the final, published document. See http:/www.minsocam.org or GeoscienceWorld

biotite and amphibole at relatively high concentrations and for determining any interactions with potential saline aqueous fluids. Yet, there are few studies on the incorporation of Cl in amphibole and biotite in high-grade iron-formation rocks (e.g. Henry 1988; Zhu et al. 1994; Daigle 2015). This paper examines Cl-rich amphibole and biotite in Archean granulite-facies iron-formation rocks from the Beartooth Mountains, Montana, USA to establish some of the crystallographic constraints and metamorphic fluid relations that serve as driving forces enhancing Cl incorporation in these minerals.

GEOLOGIC AND PETROLOGIC SETTING

The Beartooth Mountains represent a portion of one of several exposures of Archean rocks that make up the northern part of the Wyoming Province of North America (Mueller et al. 2014). The northern Wyoming Province has two primary subdivisions: (1) the Beartooth-Bighorn magmatic zone (BBMZ) composed predominantly of Mesoarchean (2.8-2.9 Ga) metaplutonic rocks of the tonalite-trondhjemite-granodiorite (TTG) association with enclaves of older (up to 3.5 Ga) lithologies and (2) the Montana metasedimentary terrane (MMT) containing a variety of Neoarchean metasedimentary rocks interspersed with older 3.2-3.5 Ga gneisses (Mueller et al. 1985, 1993, 2008, 2014; Mueller and Frost 2006).

The Beartooth Mountains can be divided into four major blocks based on distinct geologic characteristics (Fig. 1). The Stillwater Block is typified by the 2.7 Ga Stillwater Layered Igneous Complex and its associated contact-metamorphic aureole; and the North Snowy Block has an interlayered series of lithologies of variable age characteristic of the MMT (Mogk and Henry 1988). The South Snowy Block and Beartooth Plateau Block are lithologically dominated by 2.8 Ga Mesoarchean TTG plutonic and metaplutonic igneous rocks typical of the BBMZ. These two blocks have been interpreted as exposures of continental crust developed by a Mesoarchean

Always consult and cite the final, published document. See http:/www.minsocam.org or GeoscienceWorld

marginal arc built on Hadean-Eoarchean crust (Mueller et al. 2014). The western portion of the South Snowy Block is considered to be part of a shallower Mesoarchean crustal section (10-15 km depth) in which 2.8 Ga mildly-to-undeformed plutons cut a thick sequence of metamorphosed turbidites, quartzites, shales and iron-formation units – the Jardine Metasedimentary Sequence (JMS, Fig. 1). In contrast, the Beartooth Plateau Block, the area of interest for this study, is a deeper section of Mesoarchean continental crust (20-25 km depth) in which deformed (meta)plutonic rocks exhibit mutually cross-cutting relations among all of the plutonic lithologies i.e. they are multiple, independent magmatic units mixed ductilely in the middle crust (Henry et al. 2014, Mueller et al. 2014).

The Beartooth Plateau Block is typified by the 2.79-2.83 Ga Long Lake magmatic complex (LLMC, Fig. 1) comprised of a diverse assemblage of rocks ranging from amphibolites and amphibole-bearing gneisses of dioritic/tonalitic composition to more evolved TTG-suite rocks that range from granite to granodiorite to trondhjemite (Mueller et al. 2010). The source regions of individual magma bodies in the LLMC likely ranged from lithospheric mantle to mid-crustal levels (Mueller et al. 2014). Felsic and more mafic metaplutonic rocks of the TTG suite have calc-alkaline affinities and geochemical traits similar to magmas derived from modern arcs. The LLMC contains xenoliths of older (up to 3.5 Ga), high-grade, metamorphic rocks, some of which contain detrital zircons as old as 4.0 Ga (Mueller et al. 1998, Valley et al. 2005, Mueller and Wooden 2012, Henry et al. 2014, 2015).

Xenolithic supracrustal, ultramafic and mafic igneous rocks of varying size having medium-to-high-grade metamorphic overprints are particularly abundant in the pink granitic and gray granodioritic rocks of the easternmost Beartooth Mountains (Henry et al. 1982, 2014, 2015). The metamorphosed supracrustal lithologies include quartzite, metapelitic gneiss/migmatite and meta-

Always consult and cite the final, published document. See http:/www.minsocam.org or GeoscienceWorld

iron-formation. Multiple stages of metamorphism are exhibited by the xenolithic rocks. The metamorphic overprints include a locally preserved granulite-facies metamorphism (M1; 775-800°C, 6-8 kbar), an extensive amphibolite-facies overprint (M2; 650-680 C, 6-8 kbar), small-scale granulite-facies dehydration proximal to trondhjemitic veins (M3; 750 C, 6 kbar), and greenschist facies alteration associated with late fracture and grain rim alteration (e.g., Henry et al. 1982; Mueller et al. 2010, 2014; Henry et al. 2014, 2015; Daigle 2015).

Iron-formation xenoliths are typically relatively small (2-4 m) blocks or layers. They can be found as blocks in the LLMC granitic and granodioritic gneisses, boudinaged within high-temperature mélanges (Fig. 2) or ductilely folded with other lithologies (e.g. Rowan 1969). A garnet-biotitite reaction zone between an iron-formation boudin and proximal tonalitic gneiss yields formation temperatures of reaction zones at ~740°C and is indicative of high-temperature assembly of the mélange (Henry et al. 2014). Locally, high concentrations of Cl has been found in amphibole and biotite in the granulite-facies iron-formations of the eastern Beartooth Mountains (Henry et al. 1982; Henry 1988; Daigle 2015).

ANALYTICAL AND NORMALIZATION PROCEDURES

Amphibole, biotite, orthopyroxene, clinopyroxene, garnet and plagioclase were quantitatively analyzed by wavelength-dispersive spectrometry (WDS) using the JEOL 733 electron microprobe (EPMA) at Louisiana State University. WDS analyses were done with an accelerating potential of 15 kV and a beam current of 10-15 nA using a 2 μm electron-beam diameter for most minerals. Counting times for the major elements was typically 30-40 seconds on the peaks and 20-30 seconds on the backgrounds and for the minor and trace elements was typically 60 seconds on the peaks and 30-40 seconds on the backgrounds. Because of the potential overlap of F Kα with Fe L peak, a WDS scan was done over of the F peak location to establish the smallest offsets for

Always consult and cite the final, published document. See http:/www.minsocam.org or GeoscienceWorld

optimal background measurements of F. Clinopyroxene commonly contains very-fine exsolution lamellae of orthopyroxene so a reintegrated composition was obtained by doing a traverse perpendicular to the exsolution lamellae using a 10 μm rastered beam area. Standards used were well-characterized synthetic and natural minerals. For amphibole and biotite, the standards included andalusite (Al), diopside (Ca, Mg, Si), fayalite (Fe), chromite (Cr), kaersutite (Ti), rhodonite (Mn), albite (Na), sanidine (K, Ba), tugtupite (Cl), and apatite (F). For pyroxene the standards were andalusite (Al), diopside (Ca, Mg, Si), hypersthene (Fe), chromite (Cr), kaersutite (Ti), rhodonite (Mn), albite (Na), and sanidine (K). Garnet standards were almandine (Si, Al, Fe), pyrope (Mg), grossular (Ca), rhodonite (Mn), chromite (Cr), and kaersutite (Ti). For feldspar these standards included albite (Na, Si), plagioclase (Al, Ca), sanidine (K, Ba), and kaersutite (Mg, Fe). On the basis of replicate analyses of secondary standards, analytical precision for selected oxides is estimated to be ± 0.11% SiO_2, ± 0.32% Al_2O_3, ± 0.07% TiO_2, ± 0.05% FeO, ± 0.09% MgO, ± 0.02% CaO and ± 0.04% Na_2O, BaO, MnO. Minimum detection limits for selected low-concentration oxides and elements were determined to be 0.03% for MnO, Cr_2O_3, FeO, MgO, Cl, and to be 0.07% for BaO and F.

Normalization procedures for the analytical data followed several approaches to optimize the mineral chemical information. Feldspar formulae were normalized on the basis of 8 oxygens with all Fe reported as FeO. Garnet and pyroxene were normalized on the basis of 12 and 6 oxygens, respectively, and the Fe^{3+} is calculated by charge balance assuming the fixed charge associated with respective number of oxygens. For the purpose of plotting, pyroxene compositions are renormalized to the pyroxene quadrilateral components wollastonite (wo), enstatite (en) and ferrosilite (fs) after taking out the non-quadrilateral components such as Mg-tschermaks, kanoite, etc., and these are generally <10% of the components in the iron-formation pyroxenes. Because of

Always consult and cite the final, published document. See http:/www.minsocam.org or GeoscienceWorld

the presence of magnetite in all samples, it is assumed that biotite $Fe^{3+}/Fe_{total} = 0.22$ (based on Mössbauer studies of Dyar 1987; Guidotti and Dyar 1991). Normalization of biotite is done on the basis of 24 anions. Biotite from high-grade metamorphic rocks typically exhibit a systematic deprotonation related to Ti substitution in accordance with the substitution (Fe^{2+}, Mg, Mn^{2+}) + 2 $OH^- = Ti + 2\ O^{2-}$ (Henry et al. 2005). As such, the amount of deprotonation is calculated using the relation $O^{2-} = 2$ Ti. Amphibole was normalized using the average of several normalization schemes and classified using the procedure of Locock (2014) for the most recent amphibole classification schemes (Hawthorne et al. 2012). Consistent with the recommendation of Hawthorne et al. (2012), it is assumed that deprotonation of the W anion is similar to the Ti-substitution reaction in biotite and is calculated using the relation $^{W}O = 2$ Ti. None of the amphiboles and biotite are Cl-dominant (i.e. chloro-species), but the term "Cl-rich" is used here as a prefix for those amphiboles and biotites with >0.5 Cl apfu. Supplemental Data Tables S1-S5 contain EPMA data and normalized mineral formulae for representative or averaged values of pyroxene, garnet, feldspar, amphibole and biotite in the samples used for this study.

RESULTS

The iron-formation samples of the eastern Beartooth Mountains generally exhibit textures and mineral assemblages consistent with M1 granulite facies metamorphism, but they commonly have late fractures or partially replaced grain boundaries that represent a later, lower temperature overprint. The granulite-facies metamorphic mineral assemblages are quartz (qtz) + magnetite (mag) + orthopyroxene (opx) + garnet (grt) ± clinopyroxene (cpx) ± calcium clino-amphibole (cam) ± biotite (bt) ± plagioclase (pl). The iron-formation samples also contain trace minerals such as apatite (ap), ilmenite (ilm), zircon (zir), hercynite (hc) and tourmaline (tur) as well as alteration minerals such as ankerite (ank), siderite (sid) or grunerite (gru) in fractures and

Always consult and cite the final, published document. See http:/www.minsocam.org or GeoscienceWorld

187 grunerite or actinolite (act) partially replacing pyroxene margins. Of particular interest for this
188 study are the 14 iron-formation samples containing Cl-bearing amphibole and/or biotite
189 considered to have developed during peak metamorphism (Table 1).
190
191 **Mineralogical and textural characteristics of iron-formation samples**
192 The iron-formation lithologic units in the eastern Beartooth Mountains are massive-to-banded
193 with the banding developed on a millimeter-to-centimeter scale, primarily reflecting varying
194 modal amounts of constituent minerals. Some of the banding reflects variation in mineral modes
195 and some of the banding is related to texturally graded minerals, suggestive of inheritance from
196 original sedimentary graded bedding of the iron-formation (see also Henry et al. 1982, 2014). The
197 iron-formation samples exhibit several common mineralogical and textural features among the
198 major and minor minerals.
199 Peak-metamorphic quartz has variable grain size (0.05 mm - 4 mm), may have dimensions
200 that are equant or elongated parallel to the overall layering, can develop prismatic subgrains and
201 typically exhibits minor undulatory extinction. The quartz grains commonly have primary and
202 secondary fluid inclusions. The primary inclusions are most commonly entirely gas-filled and are
203 interpreted as CO_2 inclusions, but there are rare aqueous inclusions with a liquid, gas bubble and a
204 cubic daughter crystal (likely halite or sylvite) and these are considered to be a separate brine
205 fluid phase (Henry et al. 2015). Most samples have secondary late fluid inclusion-rich quartz
206 veins that cross-cut all high-grade minerals with these veins being associated with the localized
207 partial replacement of orthopyroxene by grunerite and magnesiosiderite, clinopyroxene by
208 actinolite, magnetite by siderite and garnet by ankerite. Henry and Sella (1993) found that
209 secondary fluid inclusions associated with these veins are comprised mostly of N_2+CO_2

Always consult and cite the final, published document. See http:/www.minsocam.org or GeoscienceWorld

inclusions with minor CO_2+CH_4 inclusions and rare aqueous-brine inclusions trapped at 350-400°C and 1-2 kbar.

The opaque minerals are dominated by magnetite (0.05-2 mm). The smaller grains generally have a subhedral cubic shape while the larger grains are subhedral-to-anhedral elongate grains and are typically found in the silicate/oxide-rich layers of well-banded samples. Associated ilmenite can appear as separate laths, but are commonly intergrown within magnetite grains. Magnetite typically contains hercynite lamellae or blebs (1-10 μm) along three mutual octahedral planes. Small grains of pyrite and chalcopyrite are included in garnet.

Orthopyroxene is the most common pyroxene present in the samples and is pleochroic light green to light pink (Table 1, Figs. 3A, 3B). Anhedral orthopyroxene grains are relatively large (0.2-3 mm), generally elongate parallel to the weak lineation and commonly have inclusions of garnet, quartz, magnetite, calcium amphibole and/or biotite. There is no evidence of exsolved clinopyroxene in the orthopyroxene. Several of the samples contain clinopyroxene (0.1-1 mm) that exhibits a very pale green pleochroism. Many of the clinopyroxene grains contain fine exsolution lamellae of orthopyroxene, and include grains of calcium amphibole, quartz and/or magnetite.

Garnet ranges from subhedral, rounded-to-oblate grains to anhedral poikiloblastic grains (0.2-3 mm). Elongation of the garnet grains is generally parallel to layering. The grains typically have inclusions of quartz, magnetite, orthopyroxene, calcium amphibole and/or biotite.

Plagioclase grains (0.1-1 mm) are uncommon relative to the other silicate minerals and, where present, are found in the magnetite-rich bands (Table 1). In plagioclase-bearing samples with abundant garnet or amphibole, plagioclase occurs adjacent to or near the garnet or amphibole. In

Always consult and cite the final, published document. See http:/www.minsocam.org or GeoscienceWorld

samples that have lesser amounts of garnet or amphibole, plagioclase tends to occur near magnetite, quartz and orthopyroxene.

The Cl-bearing calcium amphiboles and biotites are generally minor constituents in these iron-formation samples. Calcium amphiboles exhibit a characteristic brown-green to blue-green pleochroism. These amphiboles occur in both the matrix and as inclusions in pyroxene and garnet (Figs. 3A, 3B). Biotite grains are typically small (0.1-0.5 mm) and exhibit a dark brown to dark brownish-red pleochroism. Biotite grains occur as matrix minerals (near pyroxene and garnet) as well as inclusions in both pyroxene and garnet.

Sample QC82-45, a massive silicate-rich iron-formation, was chosen for a more detailed investigation because the Cl-rich amphibole and biotite display significant variations in composition and mode of occurrence. The granulite mineral assemblage, quartz + magnetite + orthopyroxene + garnet + calcium amphibole + biotite, are typically in mutual contact. Amphibole and biotite are heterogeneously distributed in the sample and are found both as inclusions within garnet and orthopyroxene, and as matrix minerals. The sample is locally cross-cut by healed quartz fractures that are associated with abundant fluid inclusions and the retrogressive mineral assemblages of grunerite, siderite, magnesiosiderite and ankerite. The biotite and amphibole in this sample were previously examined with high-resolution transmission electron microscopy (TEM), selected-area electron diffraction and X-ray emission analytical electron microscopy (AEM) (Zhu et al. 1994). The TEM-AEM investigation of the Cl-rich amphibole and biotite found that Cl is structurally incorporated homogeneously in the crystal structure of these high-grade minerals. The high-grade biotite is primarily a 1*M* polytype. TEM-AEM examination of the retrograde grunerite showed no detectible Cl, but there are intergrowths of submicrometer-sized

Always consult and cite the final, published document. See http:/www.minsocam.org or GeoscienceWorld

Cl-rich annite, Fe-rich talc, Fe-rich clinojimthompsonite, Cl-free annite and another very wide chain silicate.

Chemistry of minerals associated with Cl-bearing amphibole and biotite

Detailed compositional data for garnet, pyroxene and plagioclase coexisting with Cl-bearing amphiboles and biotites reflect the chemical environment, establish an approach to chemical equilibrium and permit examination of element partitioning among Cl-bearing amphibole and biotite with the coexisting minerals.

Orthopyroxene is the most common pyroxene found in the iron-formation samples (Table 1). It is compositionally unzoned, except for a minor increase in Mg and decrease in Fe in the outer 30 μm, where it is in contact with garnet. Considering only the interior homogeneous regions of the orthopyroxene in all samples, orthopyroxenes are Fe-rich and are best classified as ferrosilites (Supplemental Data Table S1). 4.5-11.8 mole% of the orthopyroxene solid solution has non-quadrilateral pyroxene components (mostly the Mn-component kanoite). Those samples not containing garnet or with low modal amounts of garnet have orthopyroxene with relatively higher Mn contents. Considering only the pyroxene quadrilateral components, orthopyroxene exhibits a range of compositions among samples having molar ratios of ferrosilite / (ferrosilite + enstatite) = 0.57-0.72 and wollastonite / (wollastonite + ferrosilite + enstatite) = 0.002-0.020 i.e. pyroxene quadrilateral components adjusted for non-quadrilateral components (Fig. 4).

Clinopyroxene is the less common pyroxene in the iron-formation samples (Table 1). It commonly contains very-fine (1-2 μm in width) exsolution lamellae of orthopyroxene. Reintegrated clinopyroxene compositions are intermediate Fe-Mg clinopyroxenes with a range of compositions among samples having molar ratios of ferrosilite / (ferrosilite + enstatite) = 0.41-0.53 and wollastonite / (wollastonite + ferrosilite + enstatite) = 0.423-0.474 (Supplemental Data

Always consult and cite the final, published document. See http:/www.minsocam.org or GeoscienceWorld

Table S1, Fig. 4). There are 5.0-9.0 mole% non-quadrilateral pyroxene components in the clinopyroxene, mostly the Mn-component johannsenite and Ca-tschermaks. Those samples not containing garnet or with low modal amounts of garnet have clinopyroxene with relatively higher Mn contents. The Fe^{2+} and Mg contents of clinopyroxene and orthopyroxene show systematic shifts in composition among the samples with nearly constant Fe^{2+}-Mg partitioning such that ${}^{cpx\text{-}opx}Kd_{Fe^{2+}\text{-}Mg} = {}^{cpx}(Fe^{2+}/Mg)/{}^{opx}(Fe^{2+}/Mg) = 0.57 +/- 0.03$. In other words, orthopyroxene and clinopyroxene approach chemical equilibrium and, further, orthopyroxene preferentially partitions Fe^{2+} relative to clinopyroxene to a relatively constant degree among samples.

Garnet found in the iron-formation samples is compositionally unzoned, except for a minor increase in Fe and decrease in Mg in the outer 30 μm where it is in contact with orthopyroxene. In general, garnets in iron-formation samples are Fe-rich with significant amounts of Ca and lesser amounts of Mn, Mg and Fe^{3+} (Supplemental Data Table S2). In terms of component species, the garnets exhibit a range of compositions among samples i.e. almandine = 52.0-76.8 mole%, grossular = 3.1-27.0 mole%, andradite = 0.3-6.6 mole%, spessartine = 4.3-14.6 mole% and pyrope = 4.4-13.0 mole% (Supplemental Fig. S1, Supplemental Data Table S2). The Fe^{2+} and Mg contents of garnet and orthopyroxene show systematic shifts in composition among the samples with nearly constant Fe^{2+}-Mg partitioning such that ${}^{grt\text{-}opx}Kd_{Fe^{2+}\text{-}Mg} = {}^{grt}(Fe^{2+}/Mg)/{}^{opx}(Fe^{2+}/Mg) = 4.45 +/- 0.30$. In other words, garnet preferentially partitions Fe^{2+} relative to orthopyroxene and clinopyroxene in a relatively constant manner, and they approach chemical equilibrium.

Feldspars are relatively uncommon in the iron-formation samples and, where present, they typically are concentrated in certain layers. Mineral chemical data are present for three samples. QC82-44 and QC82-48b plagioclase grains are chemically homogeneous with a composition of $Ab_{52}An_{47}Or_1$ (Supplemental Data Table S3). The feldspar relations in QC82-49b are more

Always consult and cite the final, published document. See http:/www.minsocam.org or GeoscienceWorld

complex with poikiloblastic plagioclase containing abundant inclusions of quartz and clustered, elongate grains of K-feldspar that have the appearance of exsolution from the plagioclase host. Plagioclase in QC82-49b is highly calcic ($An_{81}Ab_{19}$) and the K-feldspar is Ba-rich ($Or_{79}Cn_{11}Ab_{10}$) i.e. can be classified as a hyalophane (e.g. Henry et al. 2015).

Chemistry of Cl-bearing amphibole and biotite

Amphibole. The Cl-bearing amphiboles associated with peak metamorphism in the 13 amphibole-bearing iron-formation samples are calcic and exhibit a significant range in composition. The amphiboles include a variety of species: magnesio-ferri-hornblende, ferro-ferri-hornblende, hastingsite, potassic hastingsite and Cl-rich potassic hastingsite (Supplemental Data Table S4). In general, these amphiboles contain significant amounts of tetrahedral ^{T}Al, octahedral $^{C}Fe^{3+}$ and ^{C}Al, eight-fold ^{B}Ca, as well as twelve-fold ^{A}Na with variable ^{A}K. Among the C cations there is substantial Fe^{2+}-Mg variability among the samples such that $^{C}Fe^{2+}$ = 1.32-2.97 apfu and ^{C}Mg = 0.72-2.45 apfu with these cations exhibiting a mutually inverse relation consistent with the exchange vector $^{C}Fe^{2+}(^{C}Mg)_{-1}$ (Fig. 5A).

Incorporation of Cl into these amphiboles is relatively systematic such that, after a threshold value is attained, Cl increases significantly with an increase of $^{C}X_{Fe2+}$ (= $^{C}Fe^{2+}/(^{C}Fe^{2+}+^{C}Mg)$), ^{A}K and ^{T}Al (Figs. 5B, 5C and 5D). Figure 5B illustrates that amphiboles with $^{C}X_{Fe2+} < 0.5$ have very small amounts of Cl (<0.04 apfu). Above the $^{C}X_{Fe2+} = 0.5$ threshold value, the maximal Cl contents increase as a function of $^{C}X_{Fe2+}$ and reach up to 0.80 Cl apfu at $^{C}X_{Fe2+} = 0.76$. A similar relationship has been recognized in other studies, e.g. a linear fit to the Cl-bearing amphibole data of Castelli (1988) plotted in Fig. 5B shows a trend very similar to this study. Of note is that Cl contents of some amphiboles do fall below or to the right of the trends defined by maximal Cl contents for a given $^{C}X_{Fe2+}$ such that a direct link among Cl with $^{C}X_{Fe2+}$, ^{A}K and ^{T}Al is not

Always consult and cite the final, published document. See http:/www.minsocam.org or GeoscienceWorld

absolute i.e. other factors may produce Cl-poorer amphiboles. The threshold values for ^{A}K is ~0.2 apfu and for ^{T}Al is ~1.6 apfu such that the Cl contents can be significantly higher in amphiboles containing the cations above these values (Figs. 5C, 5D).

Cl-bearing amphiboles exhibit a few coupled substitutions that apparently lead to the threshold compositional relations that make significant Cl incorporation in the amphibole structure permissible. In addition to the Fe^{2+} for Mg substitution among the C cations, those amphiboles with <0.2 ^{A}K apfu appear to exhibit compositional variations consistent with the exchange vector $(^{C}Al^{T}Al)(^{C}RSi)_{-1}$, where R represents the sum of the divalent cations on the C site, and those Cl-richer amphiboles with >0.2 ^{A}K exhibit compositional variations consistent with the exchange vector $(^{A}K^{T}Al)(^{A}\square Si)_{-1}$ (Fig. 6A). Both of those substitutions lead to significant increase in ^{T}Al with the latter substitution reflecting an increase in ^{A}K in the amphibole structure.

The Fe^{2+}-Mg element partitioning between amphibole and orthopyroxene in these essentially isothermal samples provide fundamental insights about the changing crystallographic environment of the octahedral sites in amphibole as the compositions change. If the environment of the crystallographic sites that incorporate Fe^{2+} and Mg is unchanged among coexisting phases, the partition coefficients between phases will be approximately constant at near-isothermal conditions. In the iron-formation samples, this is true between orthopyroxene and clinopyroxene and between orthopyroxene and garnet (see above). In the case of the amphibole-orthopyroxene partitioning, there is a significant increase in $^{cam\text{-}opx}Kd_{Fe2+\text{-}Mg}$ from ~0.45 to 0.7 for the low Cl (<0.05 apfu) and ^{A}K (<0.2 apfu) amphibole with progressive operation of $(^{C}Al^{T}Al)(^{C}RSi)_{-1}$ exchange (Figs. 6A and 6B). This change in Kd is increased even further to 0.7-1.6 with increased incorporation of Cl and ^{A}K in the amphibole structure. It indicates that partitioning of Fe^{2+} into the octahedral sites of amphibole profoundly changes such that they are progressively more

Always consult and cite the final, published document. See http:/www.minsocam.org or GeoscienceWorld

346 favorable sites for Fe^{2+}, and this is accompanied by ^{T}Al, ^{A}K and Cl increase. The deviation of the
347 amphibole inclusion data from the linear fit of the matrix data can be explained by noting that the
348 higher-Cl amphiboles have Kd > 1 so that Fe^{2+} and Mg diffusional exchange is more likely to
349 continue between included amphibole and host orthopyroxene after the peak metamorphism and
350 result in dispersion of the amphibole compositions to higher Fe^{2+} contents for a given Cl content.
351 This is analogous to the continued Mg-Fe exchange between included biotite and host garnet that
352 continues until the blocking temperature is reached for this exchange.

353 **Biotite.** Biotite grains in the two biotite-bearing iron-formation samples are notably rich in
354 Fe^{2+}, Ti, Cl, ^{T}Al and Ba (Supplemental Data Table S5). The biotite $Fe^{2+}/(Fe^{2+}+Mg)$ ratios are
355 high, in the range of 0.64 to 0.84, with biotites from QC82-45 having $Fe^{2+}/(Fe^{2+}+Mg)$ ratios
356 >0.75. Cl concentrations are significantly elevated with 0.44-1.01 Cl apfu. There is a general
357 positive correlation between Cl and $Fe^{2+}/(Fe^{2+}+Mg)$ ratios in QC82-45, but there is significant
358 dispersion of the data in the different modes of occurrence (Fig. 7A) making it difficult to identify
359 a clear correlation. Ti has notably high concentrations in sample QC82-45 with 0.54 – 0.89 apfu
360 Ti. The variation of Ti is inversely related to R (sum of Fe^{2+} + Mg + Mn) in a 1:1 relationship
361 consistent with the exchange vector $TiO_2(R(OH)_2)_{-1}$. This vector is the basis for estimation of the
362 amount of deprotonation in biotite (see analytical and normalization procedures). Ba
363 concentrations are particularly high with 0.12-0.75 Ba apfu – the upper value is close to the
364 amount necessary to be classified as a brittle mica. Further, Ba is positively correlated with Cl in a
365 roughly 1:1 relationship (Fig. 7B). Tetrahedral Al is also relatively high with 2.53-2.98 apfu and
366 is positively correlated with Cl in a very similar manner as Ba (Fig. 7C). A Ba + ^{T}Al vs. K + Si
367 plot shows a strong inverse 1:1 relationship indicative that substitution on the 12-fold and
368 tetrahedral sites is primarily consistent with the exchange vector $(Ba^{T}Al)(KSi)_{-1}$ (Fig. 7D).

Always consult and cite the final, published document. See http:/www.minsocam.org or GeoscienceWorld

Fe^{2+}-Mg element partitioning between Cl-bearing biotite and orthopyroxene in these two samples is somewhat different, but there is a common feature – Fe^{2+} partitions preferentially into biotite over orthopyroxene. The biotite-orthopyroxene partitioning ($^{bt\text{-}opx}Kd_{Fe2+\text{-}Mg}$) is 1.29 for QC81-113, 1.95 for QC82-45-matrix average and 1.82 for the average biotite included in orthopyroxene. There is a general increase in Kd as a function of Cl contents, but it is not as well expressed as for amphibole (Fig. 6B).

DISCUSSION

The incorporation of Cl into the amphiboles and biotites of the iron-formation rocks of the eastern Beartooth Mountains can be best understood by considering a combination of crystallographic constraints and the interaction with high-grade metamorphic fluids.

Crystallochemical influence on Cl contents

One of the greatest obstacles to substituting significant amounts of Cl^- into the crystal structure of amphibole and biotite is the large anionic radius of Cl^-. Assuming the anions are [3]-coordinated, the anionic radius of Cl^- is 1.81Å and is >30% larger than the anionic radii of OH^- (1.34Å), F^- (1.30Å) and O^{2-}(1.36Å). These anions occur on specific sites in amphibole (W-group anions in the *O*(3) site of amphibole) and biotite (X-group anions in the *O*(4) site of biotite) and they are bonded to octahedral cations in their respective structures. It has long been recognized that Mg-rich amphiboles and biotites can contain large amounts of F^- with little or no Cl^-, and conversely, amphiboles and biotites that are Fe^{2+}-rich can contain large amounts of Cl^- with little or no F^-. This observation, commonly termed Mg-Cl^- and Fe-F^- avoidance (see Ramberg 1952), implies that there is a significant crystallochemical influence on the anions that can be accommodated in amphibole and biotite.

Always consult and cite the final, published document. See http:/www.minsocam.org or GeoscienceWorld

Amphibole. In calcium amphiboles there are crystallochemical mechanisms that can increase the size of the *O*(3) anion site and, consequently, they enhance the probability for Cl^- substitution. C-group cations occupy three distinct crystallographic sites: *M*(1), *M*(2) and *M*(3) (Fig. 8A). These sites are arrayed as a band of edge-sharing octahedra that extend in the c direction (e.g. Hawthorne and Oberti 2007). These cations are bonded to a double chain of tetrahedra that contain T-group cations. At the junction between the octahedral and tetrahedral chains is the eight-coordinated *M*(4) site that contains the B-group cations. Below and near the center of the hexagonal ring of tetrahedra is the twelve-coordinated *A* site that accommodates the A-group cations. Of significance for Cl^- incorporation is that the *O*(3) anion site is bonded to the *M*(1) and *M*(3) octahedra. Where Cl^- is present in the *O*(3) site there is displacement of the site effectively influencing the *A* site sitting above and below the tetrahedral bands such that ^{A}K bonds more effectively with Cl^- (e.g. Oberti et al. 1993, Hawthorne and Oberti 2007). As such, substitutions that increase the size of these octahedral sites will expand the *O*(3) site size. Fe^{2+} and Mg are preferentially incorporated into the *M*(1) and *M*(3) sites, whereas octahedral Al, Fe^{3+}, and Ti are preferentially accommodated in the *M*(2) site with the remainder of the site typically occupied by Mg. The substitution of Fe^{2+} for Mg on the *M*(1) and *M*(3) sites effectively enlarges the *O*(3) site and results in favorable incorporation of ^{T}Al and $^{A}(Na,K)$ into the amphibole (Hawthorne and Oberti 2007). The substitution of ^{T}Al for Si serves to enlarge the double chains of tetrahedra (e.g. Oberti et al. 1993, 1995)

With these crystallochemical influences in mind, the systematics of the amphiboles from the iron-formation samples of the eastern Beartooth Mountains can be further considered. Substitution of Fe^{2+} for Mg is clearly in accordance with the $^{C}Fe^{2+}(^{C}Mg)_{-1}$ exchange vector (Fig. 5A). Where a threshold value of $^{C}X_{Fe2+} = 0.5$ is attained, Cl contents in the calcium amphibole can

Always consult and cite the final, published document. See http:/www.minsocam.org or GeoscienceWorld

414 increase (Fig. 5B). There are also threshold levels of ~0.2 apfu ^{A}K and 1.6 apfu ^{T}Al that should
415 be attained before Cl contents are observed to increase significantly (Figs. 5C, 5D). The positive
416 relationship of K and Cl above the K threshold value likely reflects the mutual bonding influence
417 inherent in the crystallochemical relations (Oberti et al. 1993, Hawthorne and Oberti 2007). In
418 terms of exchange vectors, $(^{C}Al^{T}Al)(^{C}RSi)_{-1}$ is operative until a threshold level of 1.6 apfu ^{T}Al is
419 reached and this coincides with the $^{C}X_{Fe2+}$ threshold of 0.5 (Figs. 5B, 5D and 6A). At that
420 compositional limit the $(^{A}K^{T}Al)(^{A}\square Si)_{-1}$ exchange vector becomes operative and the maximal Cl
421 values track the increase of $^{C}Fe^{2+}$ (Figs. 5B, 5c and 6A). The trends of maximal Cl contents
422 suggest that there may be Cl-saturation concentrations for these amphiboles at their formation
423 pressure and temperature conditions, and that the saturation levels are likely controlled by a
424 combination of crystallochemical factors and fluid compositions. Comparable maximal Cl
425 relations are found in the extensive terrestrial and extraterrestrial amphibole dataset of Giesting
426 and Filiberto (2016, Fig. 2).

427 A noteworthy relationship is that the $^{C}Fe^{2+}$-Mg partition coefficient changes as a function of
428 Cl contents (and ^{T}Al) such that the calcium amphibole more effectively partitions Fe^{2+} than
429 coexisting orthopyroxene as ^{T}Al and Cl increase (Fig. 6B). The implication is that an increase in
430 ^{T}Al, related to bulk composition or increase in metamorphic grade, and/or to the amount of Cl^{-} in
431 a coexisting fluid phase, will enhance the partitioning of Fe^{2+} into calcium amphibole. In turn, this
432 can set up a feedback mechanism such that the more Cl available from a fluid the more Fe^{2+}-rich
433 the amphibole can become, and this produces a crystal structure that can accommodate more Cl
434 which makes this amphibole more favorable for Fe^{2+} incorporation, and the cycle continues until
435 Cl saturation is reached or aqueous Cl^{-} is fully equilibrated with the amphibole.

Always consult and cite the final, published document. See http:/www.minsocam.org or GeoscienceWorld

436 **Biotite.** Cl incorporation into the *O*(4) anionic site of biotite is similarly constrained by the
437 relatively large anionic radius of Cl such that crystallographic mechanisms that enlarge this site
438 enhance the probability for Cl substitution. Biotite has a basic sandwich-like structure in which
439 there are two layers of cations in tetrahedral coordination (T-group cations; Si, Al or Fe^{3+}) with
440 the apices opposing each other and an intervening layer of octahedrally coordinated cations (M-
441 group cations) or vacancy (Fig. 8B). M-group cations or vacancies are accommodated in either
442 the *M*(1) or *M*(2) octahedral sites with vacancies or lower-charged cations favoring *M*(1)
443 occupancy (Brigatti and Guggenheim 2002). The tetrahedral-octahedral-tetrahedral unit is
444 negatively charged and the biotite structure is charge-compensated by incorporation of relatively
445 large, ditrigonally coordinated interlayer cations (A-group cations such as K^+, Na^+, Ba^{2+} or Ca^{2+})
446 or by vacancy. Each X-group anion (OH^-, O^{2-}, F^- or Cl^-) at the *O*(4) is bonded to one *M*(1) cation
447 and two *M*(2) cations and is at the same level as the apical oxygens of the tetrahedra, but not
448 shared with the tetrahedra. Modifications in the local environment of the *O*(4) site will influence
449 the size of the site. The general observation that Cl substitution tends to be more common in Fe-
450 rich biotites suggests the increased *a* and *b* lattice dimensions associated with Fe^{2+} for Mg
451 substitution enlarges the *O*(4) site. Volfinger et al. (1985) suggested that the positive correlations
452 between Fe and Cl is related to expansion of the *O*(4) anion site and this is due to a decrease of
453 rotation of the tetrahedra to a more regular hexagonal array. However, the rotation due simply to
454 Fe^{2+} substitution alone may not be sufficient to explain the large range of Cl incorporation (e.g.
455 Kullerud 2000). Other crystallochemical factors can expand the lattice and permit enhanced Cl
456 substitution on the *O*(4) site. For example, the incorporation of additional Al in the tetrahedral site
457 will increase the T-O distance and enlarge the tetrahedral sheet, and this allows accommodation

Always consult and cite the final, published document. See http:/www.minsocam.org or GeoscienceWorld

458 of more Fe^{2+} in the octahedral sheet and expansion of the *O*(4) site (Brigatti and Guggenheim
459 2002).

460 In the two biotite-bearing iron-formation samples there are several features that relate to the
461 crystallographic features that favor Cl incorporation into biotite. (1) The Cl contents are relatively
462 high (> 0.4 apfu) in the two samples. However, for these samples there is a weak positive
463 correlation between Cl and $Fe^{2+}/(Fe^{2+}+Mg)$ ratios (Fig. 7A). (2) There is a stronger correlation
464 between Cl and Ba (Figs. 7B) within a given sample, but less so between the two samples. (3)
465 There is a strong correlation of Cl and ^{T}Al between and within samples (Fig. 7C). This implies
466 that increased ^{T}Al has a significant influence on the variability of Cl contents. In sample QC82-
467 45 Ba^{2+} probably does not significantly expand the *O*(4) site but, due to charge-balance
468 constraints, it introduces ^{T}Al into the biotite structure via the exchange vector $(Ba^{T}Al)(KSi)_{-1}$, and
469 this enlarges the tetrahedral rings and, consequently, the *O*(4) site (Fig. 7D). Tracy (1991) noted
470 that the most Ba-rich biotite from a skarn zone contains up to 1.88 apfu Ba, 2.52 apfu Cl and 3.53
471 apfu ^{T}Al. In this example the Ba and ^{T}Al incorporation is largely consistent with the
472 $(Ba^{T}Al)(KSi)_{-1}$, exchange vector, but that the tetrahedral Fe^{3+} exchange vector $(Ba^{T}Fe^{3+})(KSi)_{-1}$
473 also influences the Ba incorporation. In combination, these substitutions increase the size of the
474 tetrahedra such that Cl incorporation is even more favorable.

475 **Influence of high-grade metamorphic fluids**

476 Compositions of Cl-bearing minerals can be used to estimate the chemistry of coexisting
477 aqueous fluids. Based on the chemistry of Cl-bearing apatite in iron-formation sample QC82-45,
478 Zhu et al. (1994) used the Cl-OH apatite-fluid exchange reactions to calculate the composition of
479 the coexisting fluid. They found that, for the estimated metamorphic conditions, the metamorphic
480 fluid that interacted with the apatite was a relatively Cl-rich brine of about 4 molar Cl^{-} (or ~25

Always consult and cite the final, published document. See http:/www.minsocam.org or GeoscienceWorld

481 wt% NaCl, i.e., close to halite saturation) with a pH of 4.6. The experimental study of Munoz and
482 Swenson (1981) involving OH-Cl biotite-fluid exchange reactions for a range of X_{Fe} contents
483 resulted in a semi-quantitative expression that allows approximation of the Cl contents in aqueous
484 fluids coexisting with biotite. Application of the expression to the biotite data of this current study
485 revealed that the aqueous fluids have f_{H2O}/f_{HCl} ratios of 0.68-0.82. Taken together, these
486 calculations are indicative of a very saline aqueous fluid coexisting with the Cl-rich amphibole
487 and biotite in the granulite-facies iron-formation rocks. The aqueous fluid phase composition
488 calculations and the observations of the uncommon aqueous fluid inclusions containing cubic
489 daughter crystals coexisting with CO_2 fluid inclusions observed in the iron-formation samples
490 implies that brine-CO_2 fluid immiscibility is likely to be operative during peak metamorphism.

491 Processes that lead to brine-CO_2 fluid immiscibility in high-grade metamorphic rocks can be
492 considered by examining the H_2O-CO_2-NaCl system at relevant conditions. Experimental work
493 by Aranovich et al. (2010) allowed them to calculate updated phase diagrams for the H_2O-CO_2-
494 NaCl system. Their phase diagram, calculated at 800°C and 9 kbar, illustrates that there is a
495 prominent miscibility gap between saline aqueous fluids and CO_2-rich fluids (Fig. 9). An
496 important implication is that any mechanism that drives a single-phase aqueous fluid phase into
497 the miscibility gap results in the generation of two fluids – one that is CO_2-rich and one that is a
498 saline aqueous fluid. In the high-grade metamorphic setting of the iron formations the two most
499 likely ways to drive the fluid toward the miscibility gap is through the introduction of CO_2 or the
500 loss of H_2O from the fluid system. The first scenario, CO_2 gain, has been one of the mechanisms
501 that has been used to explain dehydration of several granulite facies terrains (e.g. Newton et al.
502 1980). As illustrated in Figure 9A, the continued introduction of CO_2 can also generate two fluid
503 phases, a CO_2 fluid that becomes an increasing proportion of the total fluid and an aqueous fluid

Always consult and cite the final, published document. See http:/www.minsocam.org or GeoscienceWorld

that becomes progressively more saline but a decreasing proportion of the total fluid phase. The second scenario, H_2O loss, can be produced by a couple of H_2O-removal mechanisms: hydration of anhydrous minerals in proximal lithologies or loss of H_2O to nearby H_2O-undersaturated silicic melts (e.g. Aranovich et al. 2014, Manning and Aranovich 2014). In either of these H_2O-loss mechanisms, most single phase aqueous fluid compositions will change such that it is driven away from the H_2O corner until it encounters the H_2O-CO_2 miscibility gap (Fig. 9B). At that point the aqueous phase will exsolve and can become highly enriched in NaCl with continued loss of H_2O.

Once a saline aqueous fluid is generated there are several further implications for the evolution of the meta-iron-formation. (1) Saline aqueous fluids have reduced wetting angles relative to CO_2 fluids (e.g. Gibert et al. 1998). As such, the saline fluids are more likely to be transported and lost to the system i.e. they have a lower likelihood of being preserved as fluid inclusions than CO_2 fluid inclusions. Accordingly, the proportions of the two types of fluid inclusions preserved will probably not reflect the proportions of these fluids at the time of unmixing. As such, determination of the driving mechanism for the specific unmixing scenario will be difficult to establish because of the differential movement and loss of these distinct fluid phases, i.e., it will generally appear to be controlled by the gain of CO_2. (2) The presence of saline aqueous fluids and CO_2 fluids reduce the activity of H_2O and tend to drive dehydration reactions forward (to lower temperatures) in the system. (3) High salinity enhances complexing in aqueous fluids, influence mineral solubilities and can preferentially extract specific cations such as LREEs in the aqueous fluids (e.g. Newton and Manning 2010, Manning and Aranovich 2014). (4) A flux of saline fluids may condition the amphibole and biotite to undergo compositional changes (e.g. increase in ^{T}Al) making them more amenable to Cl incorporation, i.e. a feedback mechanism

Always consult and cite the final, published document. See http:/www.minsocam.org or GeoscienceWorld

between fluid and mineral. This phenomenon is more likely to occur in environments of high flux of saline fluids (e.g. shear zones or hydrothermal zones), but this may be operative to a lesser extent in the meta-iron-formations (e.g. Kullerud 2000).

IMPLICATIONS

The manner in which Cl is incorporated in amphibole and biotite from the granulite-facies meta-iron-formations of the Archean terrain of the eastern Beartooth Mountains, Montana, leads to a change in perspective of the interplay between crystallographic and fluid chemical influences. In the near-isothermal, Fe-rich environment of the meta-iron-formations of this study there is a general positive relation between Fe^{2+} and Cl contents in both amphibole and biotite, but Cl incorporation is more nuanced. Ultimately, the maximal amounts of the relatively large Cl^- anion is preconditioned by the necessity to significantly expand the Cl-bearing anionic sites, *O*(3) in amphibole and *O*(4) in biotite. This appears to be partially satisfied by Fe^{2+} substitution for Mg, but there are additional influences. In amphibole there appear to be threshold values of the $^{C}Fe^{2+}/(^{C}Fe^{2+} + {}^{C}Mg)$ ratio, ^{A}K and ^{T}Al that must be attained before significant amounts of Cl are incorporated into the structure (Figs. 5B, 5C, 5D). In biotite, in addition to $Fe^{2+}/(Fe^{2+}+Mg)$, the substitution of ^{T}Al also appears to serve to expand the anionic *O*(4) site (Fig. 7C). The maximal Cl contents in amphibole appear to follow a linear trend as a function of $X^{c}Fe^{2+}$ (Fig. 5B), and is suggestive of a possible saturation concentration level of Cl constrained by the amphibole structure. However, it is uncertain whether this is a general Cl-saturation level for the amphibole structure under the restricted range of P-T conditions of these studies or is dependent on the salinity of the ambient fluid. This should be considered further experimentally (e.g. Chan et al. 2016) and in a greater diversity of geologic settings (e.g. Castelli 1988).

Always consult and cite the final, published document. See http:/www.minsocam.org or GeoscienceWorld

549 The high Cl content in the minerals of the meta-iron-formations is suggestive of a coexisting
550 high salinity aqueous fluid, but saline aqueous fluid inclusions are rare. Based on the calculations
551 using the mineral chemistry, estimations of the aqueous fluid composition indicate a Cl-rich
552 aqueous fluid (~25 wt% NaCl) and f_{H2O}/f_{HCl} ratios in the range of 0.68-0.82. However, there is
553 evidence for more abundant CO_2 fluid inclusions. As such, brine-CO_2 immiscibility is considered
554 to have been operative during peak metamorphism. A homogeneous and slightly saline aqueous
555 fluid can be driven to undergo brine-CO_2 immiscibility through the addition of CO_2 or, more
556 likely, through the loss of H_2O in the meta-iron-formation system. Because of the low
557 preservation potential of saline aqueous fluids relative to CO_2 fluids there may be scant direct
558 evidence of a saline fluid phase in high-grade rocks that may have undergone brine-CO_2
559 immiscibility. Instead, this may be implied by the presence of Cl-rich amphibole and biotite.

560 A feedback system might be considered in which the presence of Cl-rich fluids induces
561 changes in the amphibole and biotite compositions, in addition to the expected Cl-enrichment. In
562 amphibole once the threshold values for significant Cl incorporation are attained, the Fe^{2+}-Mg
563 partitioning of the amphibole and the coexisting mafic silicates changes such that the amphibole
564 more favorably partitions Fe^{2+}. This could set up a feedback such that the amphiboles will
565 become more Fe^{2+}-rich as Cl incorporates in the amphibole structure i.e. the amphibole is not just
566 a passive receptor of Cl, but changes its overall compositions in response to the fluxing saline
567 fluids in a way that accepts more Cl. This may account for some of the local Cl variations in the
568 granulite-facies meta-iron-formations considered in this study, but it will likely be more profound
569 in environments in which relatively saline fluids are fluxing through the rock system (e.g. shear
570 zones, hydrothermal environments) and may explain the occurrence of Cl-rich amphibole and
571 biotite in these settings (e.g. Kusebach et al. 2015).

Always consult and cite the final, published document. See http:/www.minsocam.org or GeoscienceWorld

ACKNOWLEDGEMENTS

The authors acknowledge thoughtful reviews and comments by David Jenkins, Sarah Penniston-Dorland and an anonymous reviewer. Barb Dutrow is thanked for insisting on retrieving some of the key samples used in this study. Financial support for this project has been provided by a number of sources: National Science Foundation - NSF EAR 0609948 (DH), LSU Campanile Charities Inc. (DH), the Red River Desk and Derrick Club (ND), New Orleans Geologic Society (ND), and the Geologic Society of America Student Research Grant (ND).

REFERENCES

Aranovich, L.Y., Makhluf, A.R., Manning, C.E., and Newton, R.C. (2014) Dehydration melting and the relationship between granites and granulites. Precambrian Research, 253, 26-37.

Aranovich, L.Y., Zakirov, I.V., Sretenskaya, N.G., and Gerya, T.V. (2010) Ternary system H_2O-CO_2-NaCl at high T-P parameters: An empirical mixing model. Geochemistry International, 48, 446-455.

Bohlen, S.R., Peacor, D.R., and Essene, E.J. (1980) Crystal chemistry of a metamorphic biotite and its significance in water barometry. American Mineralogist, 65, 55-62.

Bonin, B., and Tatu, M. (2016) Cl-rich hydrous mafic mineral assemblages in the Highiş massif, Apuseni Mountains, Romania. Mineralogy and Petrology, 110, 447-469.

Brigatti, M.F., and Guggenheim, S. (2002) Mica crystal chemistry and the influence of pressure, temperature, and solid solution on atomistic models. In Micas: Crystal Chemistry and Metamorphic Petrology (A. Mottana, F.P. Sassi, J.B. Thompson Jr. and S. Guggenheim, editors), Reviews in Mineralogy and Geochemistry, 46, 1-97.

Always consult and cite the final, published document. See http:/www.minsocam.org or GeoscienceWorld

Castelli, D. (1988) Chloropotassium ferro-pargasite from Sesia-Lanzo marbles (Western Italian Alps): a record of highly saline fluids. Rendiconti della Societa Italiana di Mineralogia e Petrologia, 43, 129-138.

Chan, A., Jenkins, D.M., and Dyar, M.D. (2016) Partitioning of chlorine between NaCl brines and ferro-pargasite: Implications for the formation of chlorine-rich amphiboles in mafic rocks. Canadian Mineralogist, 54, 337-351.

Daigle, N.M. (2015) Chlorine enrichment of hydrous minerals in Archean granulite facies ironstones from the Beartooth Mountains, Montana, USA: Implications for high-grade fluids, MS thesis, Louisiana State University, 159 pp.

Dick, L.A., and Robinson, G.W. (1979) Chlorine-bearing potassian hastingsite from a sphalerite skarn in southern Yukon. Canadian Mineralogist, 17, 25-26.

Dyar, M.D. (1987) A review of Mossbauer data on trioctahedral Micas - Evidence for tetrahedral Fe^{3+} and cation ordering. American Mineralogist, 72, 102-112.

Enami, M., Liou, L., and Bird, D.K. (1992) Cl-bearing amphibole in the Salton Sea geothermal system, California. Canadian Mineralogist, 30, 1077-1092.

Gibert, F., Guillaume, D., and Laporte, D. (1998) Importance of fluid immiscibility in the H_2O-NaCl-CO_2 system and selective CO_2 entrapment in granulites; experimental phase diagram at 5-7 kbar, 900ºC and wetting textures. European Journal of Mineralogy, 10, 1109-1123.

Giesting, P.A., and Filiberto, J. (2016) The formation environment of potassic-chloro-hastingsite in the nakhlites MIL 03346 and pairs and NWA 5790: Insights from terrestrial chloro-amphibole. Meteoritics & Planetary Science, 51, 1-27.

Guidotti, C.V., and Dyar, M.D. (1991) Ferric iron in metamorphic biotite and its petrologic and crystallochemical implications. American Mineralogist, 76, 161-175.

Always consult and cite the final, published document. See http:/www.minsocam.org or GeoscienceWorld

617 Hawthorne, F.C., and Oberti, R. (2007) Amphiboles: Crystal chemistry. Amphiboles: Crystal
618 Chemistry, Occurrence, and Health Issues, Reviews in Mineralogy and Geochemistry, 67, 1-
619 54.
620 Hawthorne, F.C., Oberti, R., Harlow, G.E., Maresch, W.V., Martin, R.F., Schumacher, J.C., and
621 Welch, M.D. (2012) Nomenclature of the amphibole supergroup. American Mineralogist, 97,
622 2031-2048.
623 Henry, D.J. (1988) Cl-rich minerals in Archean granulite facies ironstones from the Beartooth
624 Mountains, Montana, USA: Implications for fluids involved in granulite metamorphism.
625 Journal of the Geological Society of India, 31, 43-45.
626 Henry, D.J., and Sella, G.F. (1993) Late stage fractures and fluids in Archean granulite facies
627 ironstones: hydration, carbonation and ramifications. Geological Society of America Abstracts
628 with Program, 24, A158.
629 Henry, D.J., Mueller, P.A., Wooden, J.L., Warner, J.L., and Lee-Berman, R. (1982) Granulite
630 grade supracrustal assemblages of the Quad Creek area, eastern Beartooth Mountains,
631 Montana. Montana Bureau of Mines and Geology, Special Publication 84, 147-155.
632 Henry, D.J., Guidotti, C.V., and Thomson, J.A. (2005) The Ti-saturation surface for low-to-
633 medium pressure metapelitic biotites: Implications for geothermometry and Ti-substitution
634 mechanisms. American Mineralogist, 90, 316-328.
635 Henry, D.J., Mogk, D.W., and Mueller, P.A. (2014) Sequential growth of a proto-continent by
636 arc magmatism; the Paleo- to Mesoarchean record of crustal evolution in the northern
637 Wyoming Province, USA. Abstracts with Programs - Geological Society of America, 46, 283-
638 283.

Always consult and cite the final, published document. See http:/www.minsocam.org or GeoscienceWorld

639 Henry, D.J., Will, C.N., and Mueller, P.A. (2015) Ba-rich K-feldspar from mafic xenoliths with
640 Mesoarchean granitic rocks, Beartooth Mountains, Montana, USA: Indicators for barium
641 metasomatism. Canadian Mineralogist, 53, 185-198.
642 Jacobson, S.S. (1975) Dashkesanite: High-chlorine amphibole from St. Paul's rocks, Equatorial
643 Atlantic and Transcaucasia, U.S.S.R. Mineral Sciences Investigations 1972-1973, 14,
644 Smithsonian Institution Press, Washington, D.C., 17-20.
645 Jiang, S.Y., Palmer, M.R., Xue, C.J., and Li, Y.H. (1994) Halogen-rich scapolite-biotite rocks
646 from the Tongmugou Pb-Zn Deposit, Qinling, Northwestern China - Implications for the ore-
647 forming processes. Mineralogical Magazine, 58, 543-552.
648 Kamineni, D.C., Bonardi, M., and Rao, A.T. (1982) Halogen-bearing minerals from Airport Hill,
649 Visakhapatnam, India. American Mineralogist, 67, 1001-1004.
650 Krutov, G.A., and Vinogradova, R.A. (1966) Chlorohastingsite from the Odinochnoye magnetite
651 deposit, eastern Sayan. Doklady Acad. USSR. Earth Sciences Section, 169, 116-119.
652 Kullerud, K. (1995) Chlorine, titanium and barium-rich biotites - Factors controlling biotite
653 composition and the implications for garnet-biotite geothermometry. Contributions to
654 Mineralogy and Petrology, 120, 42-59.
655 Kullerud, K. (1996) Chlorine-rich amphiboles: interplay between amphibole composition and an
656 evolving fluid. European Journal of Mineralogy, 8, 355-370.
657 Kullerud, K. (2000) Occurrence and origin of Cl-rich amphibole and biotite in the Earth's crust —
658 Implications for fluid composition and evolution. In: Stober, I., Bucher, K. (Eds.),
659 Hydrogeology of Crystalline Rocks. Water Science and Technology Library. Springer
660 Netherlands, 205-225.

Always consult and cite the final, published document. See http:/www.minsocam.org or GeoscienceWorld

661 Kullerud, K., and Erambert, M. (1999) Cl-scapolite, Cl-amphibole, and plagioclase equilibria in
662 ductile shear zones at Nusfjord, Lofoten, Norway: Implications for fluid compositional
663 evolution during fluid-mineral interaction in the deep crust. Geochimica et Cosmochimica
664 Acta, 63, 3829-3844.
665 Kusebauch, C., John, T., Barnes, J.D., Klugel, A., and Austrheim, H.O. (2015) Halogen element
666 and stable chlorine isotope fractionation caused by fluid-rock interaction (Bamble Sector, SE
667 Norway). Journal of Petrology, 56, 299-324.
668 Léger, A., Rebbert, C., and Webster, J. (1996) Cl-rich biotite and amphibole from Black Rock
669 Forest, Cornwall, New York. American Mineralogist, 81, 495-504.
670 Liu, J., Liu, W., Ye, K., and Mao, Q. (2009) Chlorine-rich amphibole in Yangkou eclogite, Sulu
671 ultrahigh-pressure metamorphic terrane, China. European Journal of Mineralogy, 21, 1265-
672 1285.
673 Locock, A.J. (2014) An Excel spreadsheet to classify chemical analyses of amphiboles following
674 the IMA 2012 recommendations. Computers & Geosciences, 62, 1-11.
675 Makino, K., Tomita, K., and Suwa, K. (1993) Effect of chlorine on the crystal-structure of a
676 chlorine-rich hastingsite. Mineralogical Magazine, 57, 677-685.
677 Manning, C.E., and Aranovich, L.Y. (2014) Brines at high pressure and temperature:
678 Thermodynamic, petrologic and geochemical effects. Precambrian Research, 253, 6-16.
679 Markl, G., and Piazolo, S. (1998) Halogen-bearing minerals in syenites and high-grade marbles of
680 Dronning Maud Land, Antarctica: monitors of fluid compositional changes during late-
681 magmatic fluid-rock interaction processes. Contributions to Mineralogy and Petrology, 132,
682 246-268.

Always consult and cite the final, published document. See http:/www.minsocam.org or GeoscienceWorld

McCormick, K.A., and McDonald, A.M. (1999) Chlorine-bearing amphiboles from the Fraser mine, Sudbury, Ontario, Canada: Description and crystal chemistry. Canadian Mineralogist, 37, 1385-1403.

Mogk, D.W., and Henry, D.J. (1988) Metamorphic petrology of the northern Archean Wyoming Province, Southwestern Montana: Evidence for collisional tectonics. In Metamorphism and Crustal Evolution of the Western US (W.G. Ernst, ed.), Rubey Volume VII, Prentice-Hall, Englewood Cliffs, N.J., United States, 362-382.

Mora, C.I., and Valley, J.W. (1989) Halogen-rich scapolite and biotite - Implications for metamorphic fluid-rock interaction. American Mineralogist, 74, 721-737.

Morrison, J. (1991) Compositional constraints on the incorporation of Cl into amphiboles. American Mineralogist, 76, 1920-1930.

Mueller, P.A., and Frost, C.D. (2006) The Wyoming Province: a distinctive Archean craton in Laurentian North America. Canadian Journal of Earth Sciences 43, 1391-1397.

Mueller, P.A., and Wooden, J.L. (2012) Trace element and Lu-Hf systematics in Hadean-Archean detrital zircons: Implications for crustal evolution. Journal of Geology 120, 15-29.

Mueller, P., Wooden, J., Henry, D.J., and Bowes, D. (1985) Archean crustal evolution of the eastern Beartooth Mountains, Montana and Wyoming. The Stillwater Complex, Montana—Geology and guide: Montana Bureau of Mines and Geology Special Publication 92, 9-20.

Mueller, P.A., Shuster, R.D., Wooden, J.L., Erslev, E.A., and Bowes, D.R. (1993) Age and composition of Archean crystalline rocks from the Southern Madison Range, Montana - Implications for crustal evolution in the Wyoming Craton. Geological Society of America Bulletin, 105, 437-446.

Always consult and cite the final, published document. See http:/www.minsocam.org or GeoscienceWorld

Mueller, P.A., Wooden, J.L., Nutman, A.P., and Mogk, D.W. (1998) Early Archean crust in the northern Wyoming province - Evidence from U-Pb ages of detrital zircons. Precambrian Research, 91, 295-307.

Mueller, P.A., Mogk, D.W., Henry, D.J., Wooden, J.L., and Foster, D.A. (2008) Geologic evolution of the Beartooth Mountains: Insights from petrology and geochemistry. Northwest Geology, 37, 5-20.

Mueller, P.A., Wooden, J.L., Mogk, D.W., Henry, D.J., and Bowes, D.R. (2010) Rapid growth of an Archean continent by arc magmatism. Precambrian Research 183, 70-88.

Mueller, P.A., Mogk, D.W., Henry, D.J., Wooden, J.L., Foster, D.A. (2014) The plume to plate transition: Hadean and Archean Crustal Evolution in the Northern Wyoming Province, U.S.A. In Evolution of Archean Crust and Early Life (Y. Dilek and H. Furnes, editors), 7, 23-54, Springer Netherlands.

Munoz, J.L., and Swenson, A. (1981) Chloride-hydroxyl exchange in biotites and estimations of relative HCl/HF activities in hydrothermal fluids. Economic Geology, 76, 2212-2221.

Newton, R.C. and Manning, C.E. (2010) Role of saline fluids in deep-crustal and upper-mantle metasomatism: Insights from experimental studies, Frontiers in Geofluids. Wiley-Blackwell, pp. 58-72.

Newton, R.C., Smith, J.V., and Windley, B.F. (1980) Carbonic metamorphism, granulites and crustal growth. Nature, 288, 45-50.

Oberti, R., Ungaretti, L., Cannillo, E., and Hawthorne, F. C. (1993) The mechanism of Cl incorporation in amphibole: American Mineralogist, 78, 746-752.

Always consult and cite the final, published document. See http:/www.minsocam.org or GeoscienceWorld

726 Oberti, R., Ungaretti, L., Cannillo, E., Hawthorne, F.C., and Memmi, I. (1995) Temperature-
727 dependent Al order-disorder in the tetrahedral double-chain of C2/m amphiboles. European
728 Journal of Mineralogy, 7, 1049-1063.
729 Oen, I.S., and Lustenhouwer, W.J. (1992) Cl-rich biotite, Cl-K hornblende, and Cl-rich scapolite
730 in meta-exhalites - Nora, Bergslagen, Sweden. Economic Geology and the Bulletin of the
731 Society of Economic Geologists, 87, 1638-1648.
732 Pan, Y.M., and Fleet, M.E. (1992) Mineralogy and genesis of calc-silicates associated with
733 Archean volcanogenic massive sulfide deposits at the Manitouwadge Mining Camp, Ontario.
734 Canadian Journal of Earth Sciences, 29, 1375-1388.
735 Popp, R.K., Hibbert, H.A., and Lamb, W.M. (2006) Oxy-amphibole equilibria in Ti-bearing
736 calcic amphiboles: Experimental investigation and petrologic implications for mantle-derived
737 amphiboles. American Mineralogist, 91, 54-66.
738 Ramberg, H. (1952) Chemical bonds and distribution of cations in silicates. Journal of Geology,
739 60, 331-355.
740 Rowan, L.C. (1969) Structural geology of the Quad-Wyoming-Line Creeks area, Beartooth
741 Mountains, Montana. Geological Society of America - Memoirs, 115, 1-18.
742 Suwa, K., Enami, M., and Horiuchi, T. (1987) Chlorine-rich potassium hastingsite from West
743 Ongul Island, Lutzow-Holm Bay, East Antarctica. Mineralogical Magazine, 51, 709-714.
744 Tracy, R.J. (1991) Ba-rich micas from the Franklin Marble, Lime Crest and Sterling Hill, New-
745 Jersey. American Mineralogist, 76, 1683-1693.
746 Tsunogae, T., Osanai, Y., Owada, M., Toyoshima, T., Hokada, T., and Crowe, W.A. (2003) High
747 fluorine pargasites in ultrahigh temperature granulites from Tonagh Island in the Archean
748 Napier Complex, East Antarctica. Lithos, 70, 21-38.

Always consult and cite the final, published document. See http:/www.minsocam.org or GeoscienceWorld

749 Uher, P., Kodera, P., Lexa, J., and Bačik, P. (2014) Halogen-rich biotites from the Detva, Biely
750 Vrch Au-porphyry deposit (Slovakia): Compositional variations and genetic aspects, 4th
751 Central European Mineralogical Conference, Skalsky Dvur, 146-147.
752 Valley, J.W., Lackey, J.S., Cavosie, A.J., Clechenko, C.C., Spicuzza, M.J., Basei, M.A.S.,
753 Bindeman, I.N., Ferreira, V.P., Sial, A.N., King, E.M., Peck, W.H., Sinha, A.K., and Wei,
754 C.S. (2005) 4.4 billion years of crustal maturation: oxygen isotope ratios of magmatic zircon.
755 Contributions to Mineralogy and Petrology, 150, 561-580.
756 Vanko, D.A. (1986) High-chlorine amphiboles from oceanic rocks - Product of highly-saline
757 hydrothermal fluids. American Mineralogist, 71, 51-59.
758 Volfinger, M., Robert, M.L., Vielzeuf, D., and Neiva, A.M.R. (1985) Structural control of the
759 chlorine content of OH-bearing silicates (micas and amphiboles). Geochimica et
760 Cosmochimica Acta, 49, 37-48.
761 Whitney, D.L. and Evans, B.W. (2010) Abbreviations for names of rock-forming minerals.
762 American Mineralogist, 95, 185-187.
763 Xiao, Y.L., Hoefs, J., and Kronz, A. (2005) Compositionally zoned Cl-rich amphiboles from
764 North Dabie Shan, China: Monitor of high-pressure metamorphic fluid/rock interaction
765 processes. Lithos, 81, 279-295.
766 Zhu, C., and Sverjensky, D.A. (1991) Partitioning of F-Cl-OH between minerals and
767 hydrothermal fluids. Geochimica et Cosmochimica Acta, 55, 1837-1858.
768 Zhu, C., and Sverjensky, D.A. (1992) F-Cl-Oh Partitioning between biotite and apatite.
769 Geochimica et Cosmochimica Acta, 56, 3435-3467

Always consult and cite the final, published document. See http:/www.minsocam.org or GeoscienceWorld

770 Zhu, C., Xu, H.F., Ilton, E.S., Veblen, D.R., Henry, D.J., Tivey, M.K., and Thompson, G. (1994)
771 TEM-AEM observations of Cl-rich amphibole and biotite and possible petrologic
772 implications. American Mineralogist, 79, 909-920.
773

Always consult and cite the final, published document. See http:/www.minsocam.org or GeoscienceWorld

774 **FIGURE CAPTIONS**

775 **Figure 1.** Outline of Beartooth uplift with the major Archean blocks labeled (modified after
776 Mueller et al. 2014; Henry et al. 2015). The darker shade in the Stillwater block is the Stillwater
777 Layered Igneous Complex (2.7 Ga). The Long Lake Magmatic Complex (LLMC) and its
778 temporal equivalents occur throughout the Beartooth Plateau and South Snowy blocks. The
779 location of the iron-formation samples used in this study are in the Quad Creek (QC) and
780 Hellroaring Plateau (HR) areas. Also labeled are the Slough Creek batholith (SCB), Jardine
781 Metasedimentary Sequence (JMS), and Yellowstone River shear zone (SZ). White areas indicate
782 Phanerozoic cover. The location of the Beartooth uplift is shown in the inset of North America.

783 **Figure 2.** Boudinaged mélange of lithologies from the Quad Creek locality (Fig. 1). The iron
784 formation unit is massive-to-banded and has a high-temperature garnet-biotitite reaction zone at
785 the contact zone with the tonalitic gneiss.

786 **Figure 3**. Photomicrographs of representative iron-formation samples. (A) Mineralogical and
787 textural relations in sample QC-IS. The Cl content of a selected blue-green matrix amphibole
788 (potassic hastingsite) is shown. (B) Typical mineralogical relations in sample QC82-45. Cl
789 contents of selected inclusion and matrix amphiboles (potassic hastingsites) and biotite are shown.

790 **Figure 4.** Average compositions of interior regions orthopyroxene and reintegrated clinopyroxene
791 for 12 of the iron-formation samples plotted on a modified pyroxene quadrilateral. The lines
792 represent tie-lines connecting coexisting orthopyroxene and clinopyroxene in a single sample.
793 The gray band designates a break in the scale.

794

Always consult and cite the final, published document. See http:/www.minsocam.org or GeoscienceWorld

Figure 5. Compositional variation of Cl-bearing amphibole from 13 iron-formation samples from the eastern Beartooth Mountains, Montana. (A) Fe^{2+} vs. Mg on octahedral sites. The arrow represents the direction of the exchange vector that describes the Fe^{2+} for Mg substitution for the C cations. The solid line is a reference line with a slope of -1 and parallel to the exchange vector. (B) $^{C}Fe^{2+}/(^{C}Fe^{2+} + {}^{C}Mg)$ ratio for the octahedral sites vs. Cl. The dash-dot line is a linear fit of the Castelli (1988) data on Cl-amphiboles from impure marbles and is displayed for reference. (C) K on the A site vs. Cl. (D) Al on the tetrahedral sites vs. Cl.

Figure 6. Mineral chemical relations of amphibole and orthopyroxene of 13 iron-formation samples from the eastern Beartooth Mountains. (A) K on the twelve-fold site vs. Al on the tetrahedral sites of amphibole. There are two distinct trends to the data – below ~0.2 ^{A}K and above ~0.2 ^{A}K. The former trend is consistent with the exchange vector $(^{C}Al^{T}Al)(^{C}RSi)_{-1}$, where R = the sum of the divalent cations on the C-site, and the latter trend is consistent with the exchange vector $(^{A}K^{T}Al)(^{A}\square Si)_{-1}$. The arrow represents the direction of two exchange vectors in this composition space, but not the magnitude of the exchanges. (B) Fe^{2+}-Mg element partitioning (Kd) between amphibole and orthopyroxene vs. Cl (apfu) in amphibole in the matrix (shaded circles) and included in orthopyroxene (open circles) for all samples. The dashed line represents a linear fit of the matrix amphibole data with Cl>0.03 apfu.

Figure 7. Compositional variation of Cl-bearing biotite from two iron-formation samples from the eastern Beartooth Mountains, Montana. (A) $Fe^{2+}/(Fe^{2+}+Mg)$ vs Cl. Note the general positive relationship among the different modes of occurrence of biotite in QC82-45. (B) Ba vs. Cl. The dashed line has a slope of 1 and is used for reference. (C) Al on the T site vs. Cl. The dashed line has a slope of 1 and is used for reference. (D) Al on the T site vs. Cl. The arrow represents the

Always consult and cite the final, published document. See http:/www.minsocam.org or GeoscienceWorld

direction of the exchange vector that describes the Ba + ^{T}Al for K + Si substitution. The solid line is a reference line with a slope of -1 and parallel to the exchange vector $(Ba^{T}Al)(KSi)_{-1}$.

Figure 8. Calcium amphibole and biotite crystal structures showing the relative positions of Cl anionic site. (A) Structure of a monoclinic C2/m potassic chloro-hastingsite calculated from the crystallographic parameters of Makino et al. (1993). Projection is made onto (100) with the lower octahedral strip removed for clarity. The yellow spheres represent the anionic *O(3)* site that can be occupied by Cl^-, F^-, OH^- and/or O^{2-}. The pale peach and yellow spheres represent the *M(4)* and *A*-site cations, respectively. The gray and blue coordination polyhedral represent the tetrahedral sites (*T1* and *T2*) and the octahedral sites (*M1*, *M2* and *M3*), respectively. Note that Cl^- in *O(3)* is bonded to the *M(1)* and *M(3)* octahedral sites. (B) Structure of a monoclinic C2/c Cl-bearing intermediate Mg-Fe biotite calculated from simplified crystallographic parameters of Bohlen et al. (1980). Projection is made onto (001). The yellow spheres represent the anionic *O(4)* site that can be occupied by Cl^-, F^-, OH^- and/or O^{2-}. The gray and teal coordination polyhedral represent the tetrahedral sites (*T1* and *T2*) and the octahedral sites (*M1* and *M2*), respectively. Note that Cl^- in *O(4)* is bonded to the *M(1)* and *M(2)* octahedral sites.

Figure 9. Scenarios for generating fluid immiscibility in the H_2O-CO_2-NaCl system for high-grade metamorphic fluids. The base phase diagram was modified after the calculated diagrams of Aranovich et al. (2010). The black arrows on the sides of the miscibility gap represent the changing fluid compositions of the unmixed fluid phases. The dashed lines represent tie-lines of selected fluids in equilibrium across the miscibility gap. (A) CO_2-gain scenario. For a selected single fluid composition, designated as "x", the introduction of CO_2 causes the fluid bulk composition to move toward the CO_2 corner. Where the bulk fluid composition encounters the miscibility gap, the fluid unmixes to a CO_2-rich fluid and an H_2O-rich fluid. With further CO_2

Always consult and cite the final, published document. See http:/www.minsocam.org or GeoscienceWorld

addition the coexisting aqueous fluid becomes progressively more saline. The gray arrow within the two-fluid field is the projection of the bulk composition of the fluid as CO_2 is introduced. (B) H_2O-loss scenario. For a selected single fluid composition, designated as "x", the loss of H_2O from the system causes the fluid bulk composition to move away from the H_2O corner. Where the bulk fluid composition encounters the miscibility gap the fluid unmixes to a CO_2-rich fluid and an H_2O-rich fluid. With further loss of H_2O the aqueous fluid becomes progressively more saline. The gray arrow within the two-fluid field is the projection of the bulk composition of the fluid as H_2O is lost.

Always consult and cite the final, published document. See http:/www.minsocam.org or GeoscienceWorld

This is a preprint, the final version is subject to change, of the American Mineralogist (MSA)
Cite as Authors (Year) Title. American Mineralogist, in press.
DOI: http://dx.doi.org/10.2138/am-2018-6143

849 **TABLE**

Table 1. Iron-formation samples containing Cl-bearing calcium amphibole and/or biotite

Sample	qtz*	mag	grt	opx	cpx	cam	bt	pl	ap	zrn	tur	ilm	hc	*gru***	*act*	*sd*	*ank*
HR02-71	x	x	x	x		x				x		x	x	x		x	
QC-IS	x	x	x	x	x	x			x	x			x	x		x	x
QC-JW3	x	x	x	x	x	x							x		x		
QC81-6	x	x	x	x	x	x				x				x			
QC81-45	x	x	x	x	x	x						x	x	x			
QC81-113	x	x	x	x			x			x		x	x	x			
QC82-44	x	x		x		x		x				x				x	
QC82-45	x	x	x	x	x	x	x		x			x		x		x	x
QC82-46	x	x	x		x	x		x	x	x	x	x			x		
QC82-47	x	x		x	x	x			x	x				x			
QC82-48A	x	x	x	x	x	x		x	x	x							
QC82-48B	x	x	x			x		x	x	x							
QC82-49A	x	x		x	x	x		x	x	x							
QC82-49B	x	x	x	x	x	x		x	x	x							

850 *Abbreviations: Quartz (qtz), magnetite (mag), garnet (grt), orthopyroxene (opx), clinopyroxene (cpx), calcium
851 amphibole (cam), biotite (bt), plagioclase (pl), apatite (ap), zircon (zrn), tourmaline (tur), ilmenite (ilm),
852 hercynite (hc), grunerite (gru), actinolite (act), siderite (sd) and ankerite (ank). Mineral abbreviations are
853 consistent with the recommendations of Whitney and Evans (2010).
854 **The italicized minerals of the last 4 columns represent alteration minerals associated with fluid introduction at
855 grain boundaries and fractures indicate by late quartz veins with abundant fluid inclusions.
856

Always consult and cite the final, published document. See http:/www.minsocam.org or GeoscienceWorld

This is a preprint, the final version is subject to change, of the American Mineralogist (MSA)
Cite as Authors (Year) Title. American Mineralogist, in press.
DOI: http://dx.doi.org/10.2138/am-2018-6143

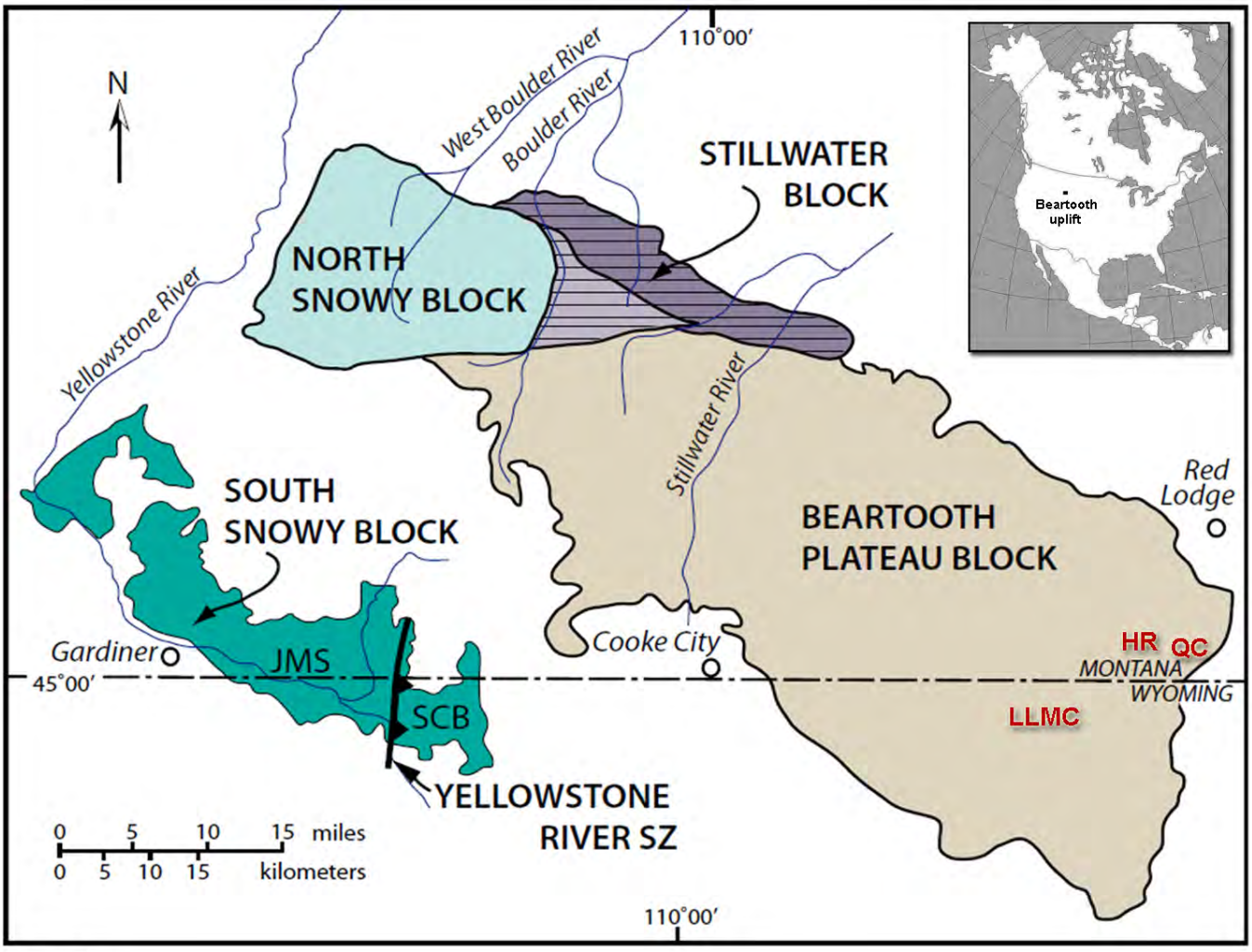

Figure 1

Always consult and cite the final, published document. See http:/www.minsocam.org or GeoscienceWorld

This is a preprint, the final version is subject to change, of the American Mineralogist (MSA)
Cite as Authors (Year) Title. American Mineralogist, in press.
DOI: http://dx.doi.org/10.2138/am-2018-6143

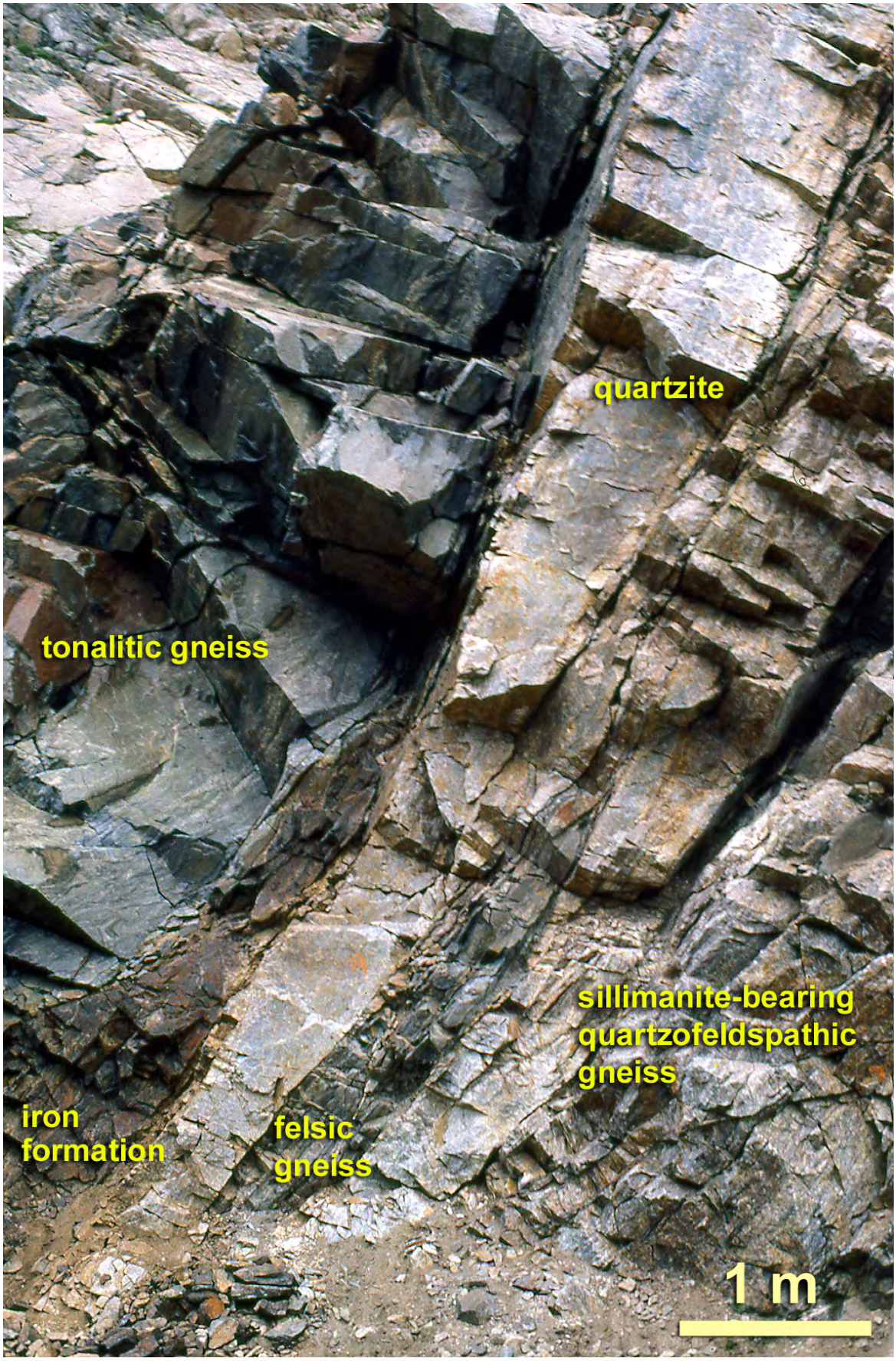

Figure 2

Always consult and cite the final, published document. See http:/www.minsocam.org or GeoscienceWorld

This is a preprint, the final version is subject to change, of the American Mineralogist (MSA)
Cite as Authors (Year) Title. American Mineralogist, in press.
DOI: http://dx.doi.org/10.2138/am-2018-6143

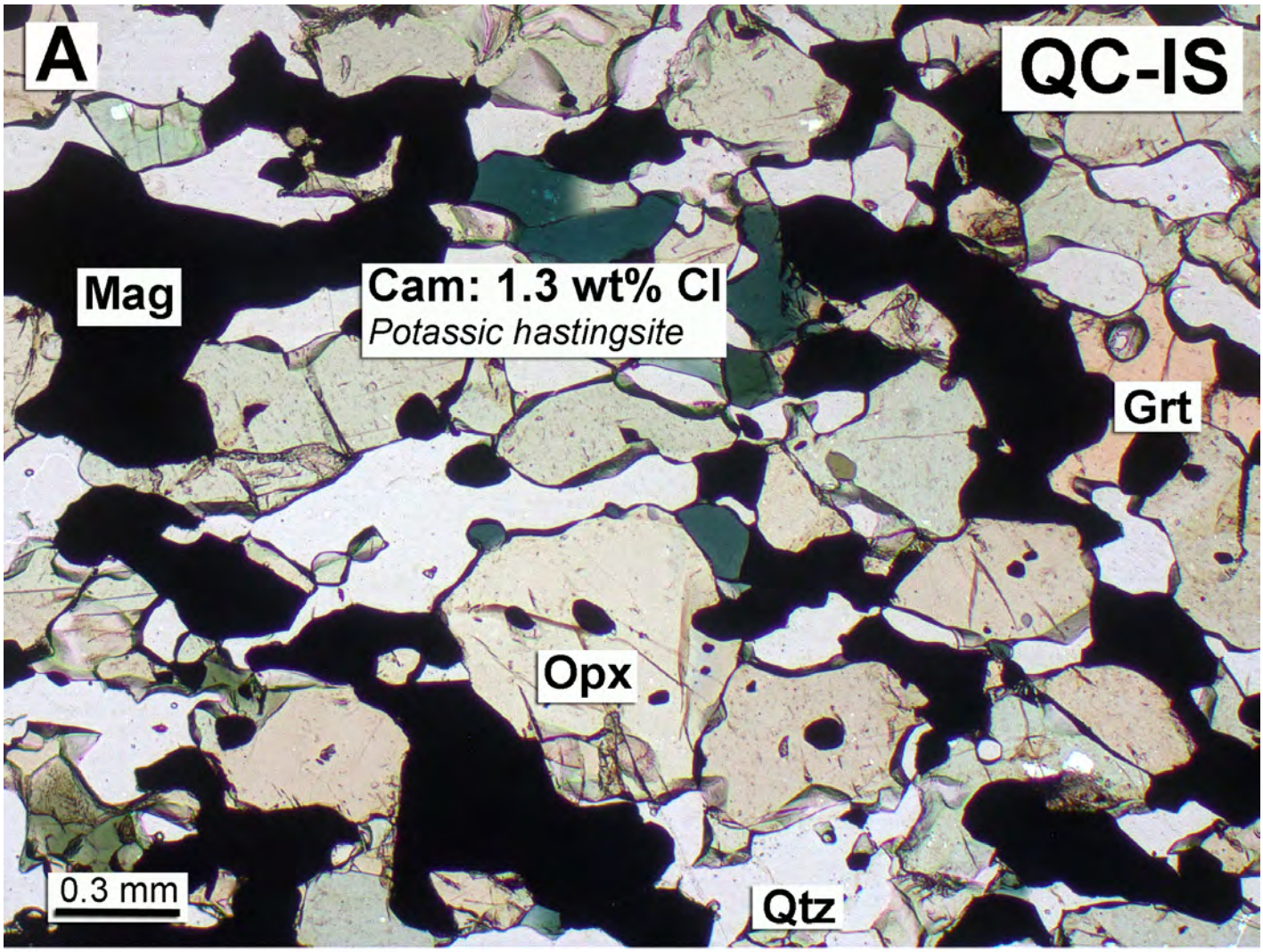

Figure 3A

Always consult and cite the final, published document. See http:/www.minsocam.org or GeoscienceWorld

This is a preprint, the final version is subject to change, of the American Mineralogist (MSA)
Cite as Authors (Year) Title. American Mineralogist, in press.
DOI: http://dx.doi.org/10.2138/am-2018-6143

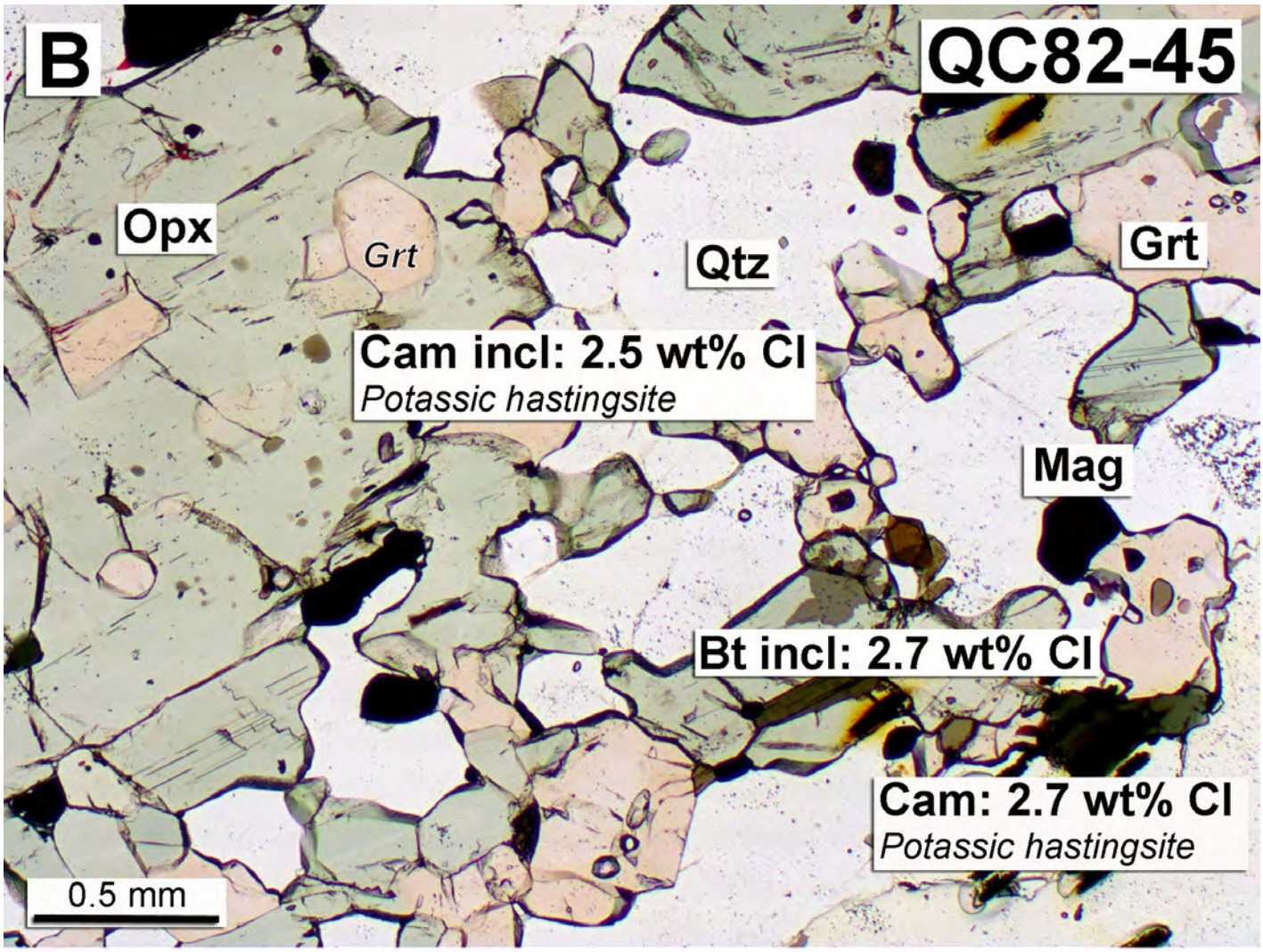

Figure 3B

Always consult and cite the final, published document. See http:/www.minsocam.org or GeoscienceWorld

This is a preprint, the final version is subject to change, of the American Mineralogist (MSA)
Cite as Authors (Year) Title. American Mineralogist, in press.
DOI: http://dx.doi.org/10.2138/am-2018-6143

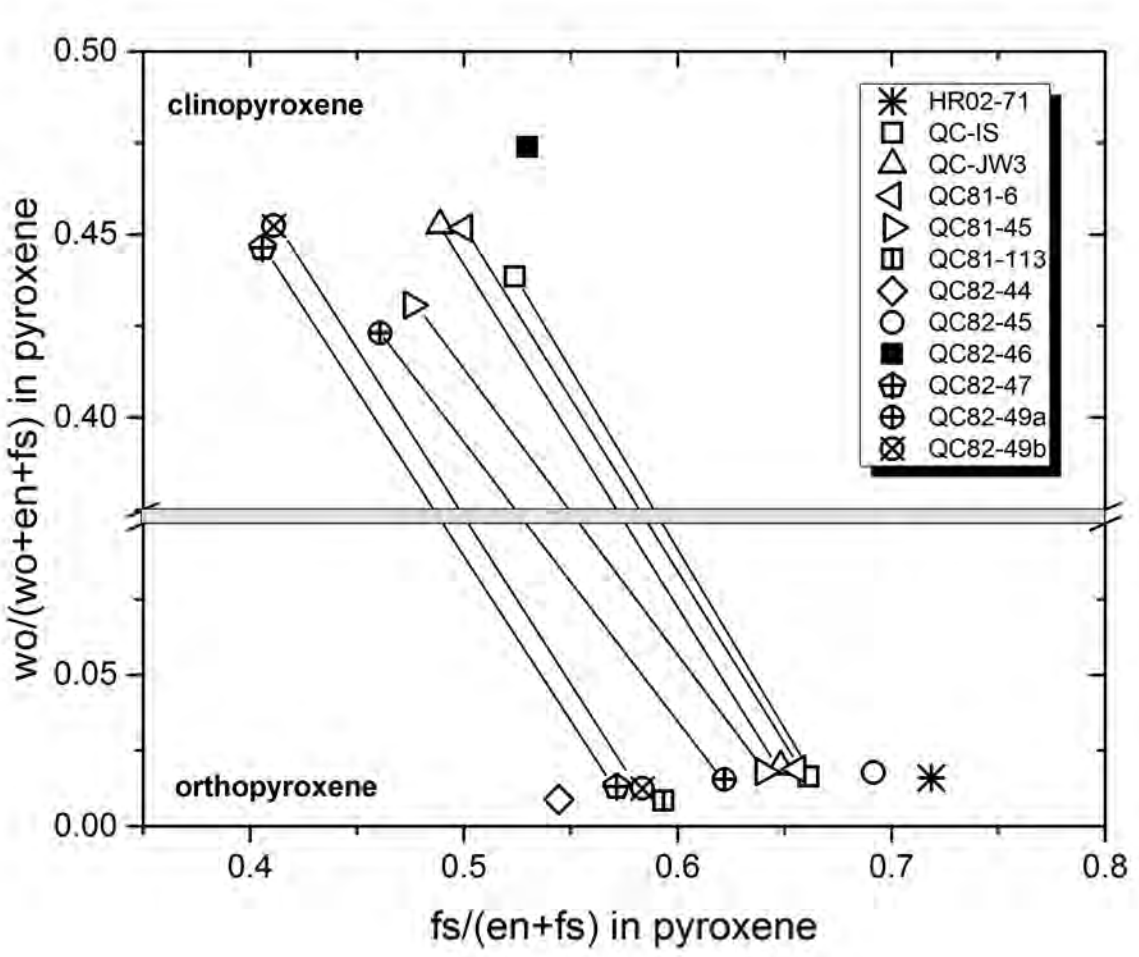

Figure 4

Always consult and cite the final, published document. See http:/www.minsocam.org or GeoscienceWorld

This is a preprint, the final version is subject to change, of the American Mineralogist (MSA)
Cite as Authors (Year) Title. American Mineralogist, in press.
DOI: http://dx.doi.org/10.2138/am-2018-6143

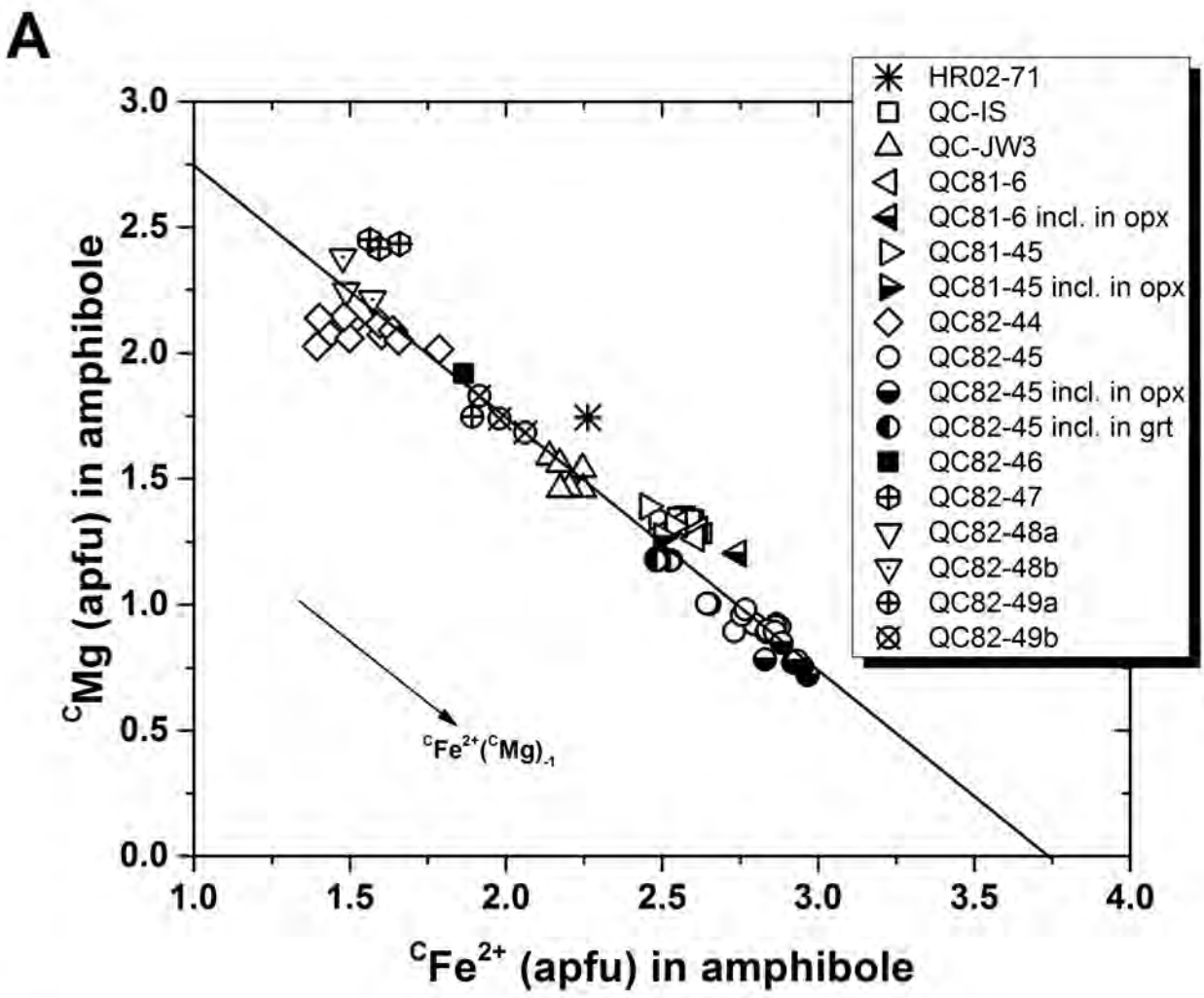

Figure 5A

Always consult and cite the final, published document. See http:/www.minsocam.org or GeoscienceWorld

This is a preprint, the final version is subject to change, of the American Mineralogist (MSA)
Cite as Authors (Year) Title. American Mineralogist, in press.
DOI: http://dx.doi.org/10.2138/am-2018-6143

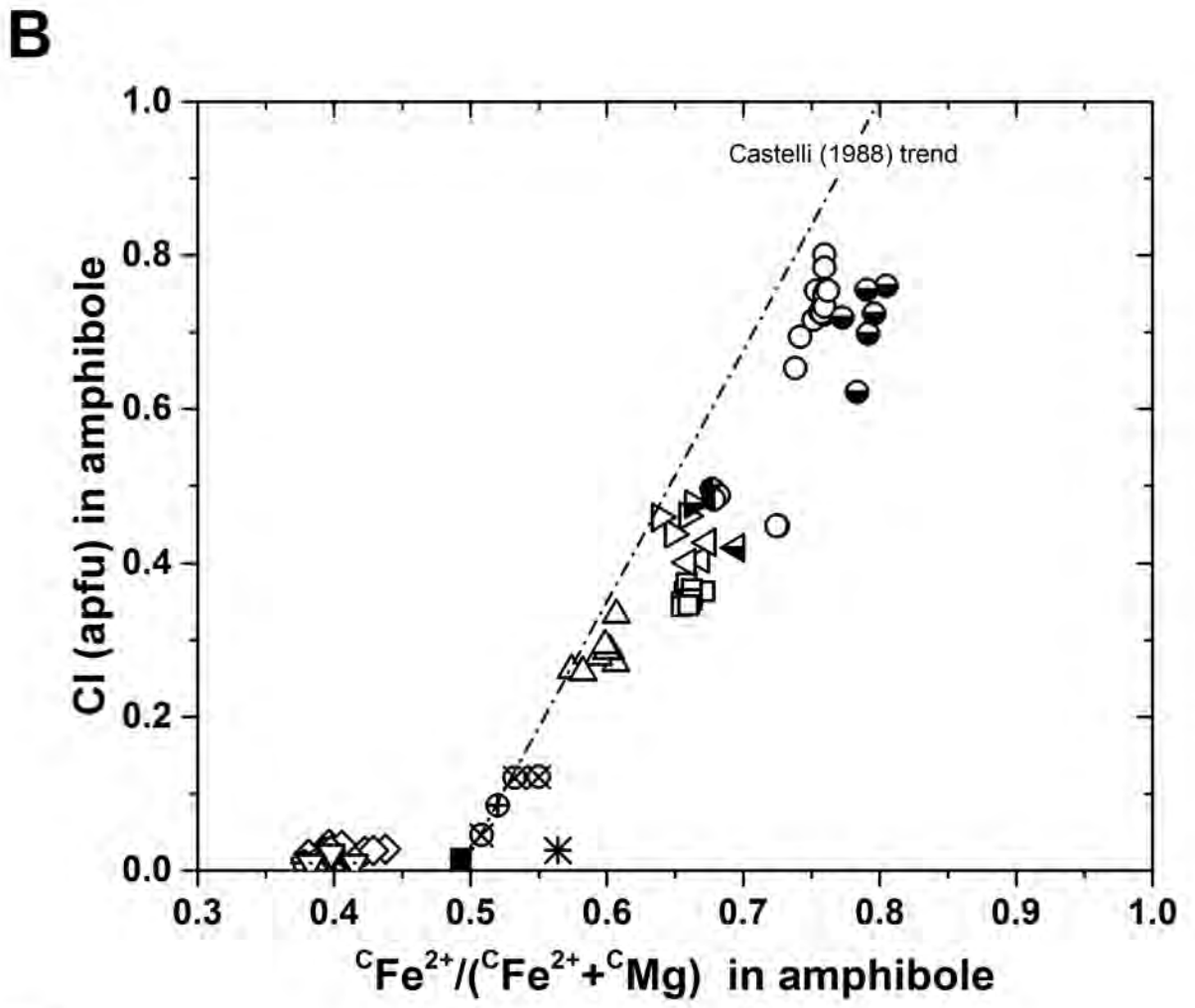

Figure 5B

Always consult and cite the final, published document. See http:/www.minsocam.org or GeoscienceWorld

This is a preprint, the final version is subject to change, of the American Mineralogist (MSA)
Cite as Authors (Year) Title. American Mineralogist, in press.
DOI: http://dx.doi.org/10.2138/am-2018-6143

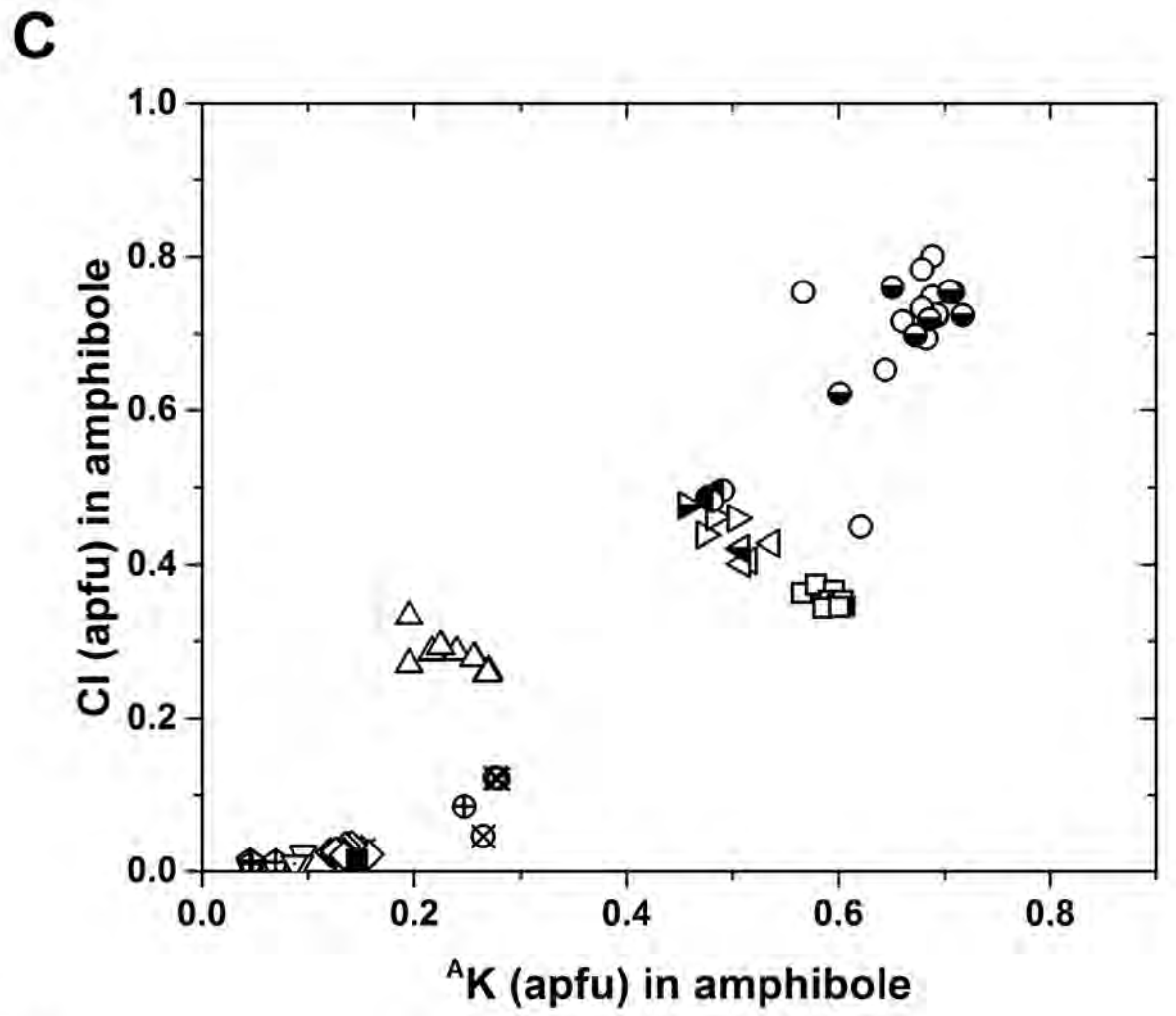

Figure 5C

Always consult and cite the final, published document. See http:/www.minsocam.org or GeoscienceWorld

This is a preprint, the final version is subject to change, of the American Mineralogist (MSA)
Cite as Authors (Year) Title. American Mineralogist, in press.
DOI: http://dx.doi.org/10.2138/am-2018-6143

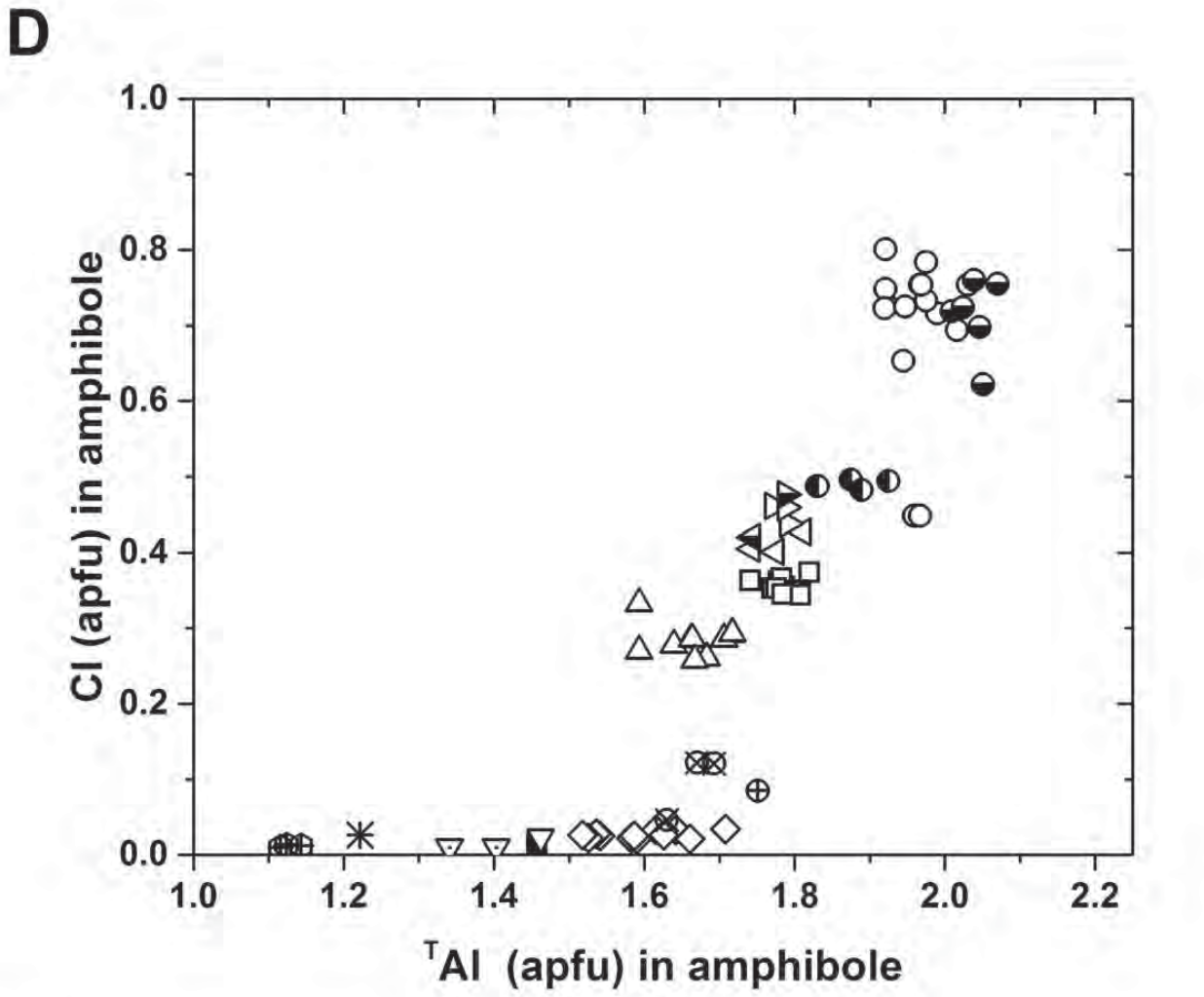

Figure 5D

Always consult and cite the final, published document. See http:/www.minsocam.org or GeoscienceWorld

This is a preprint, the final version is subject to change, of the American Mineralogist (MSA)
Cite as Authors (Year) Title. American Mineralogist, in press.
DOI: http://dx.doi.org/10.2138/am-2018-6143

A

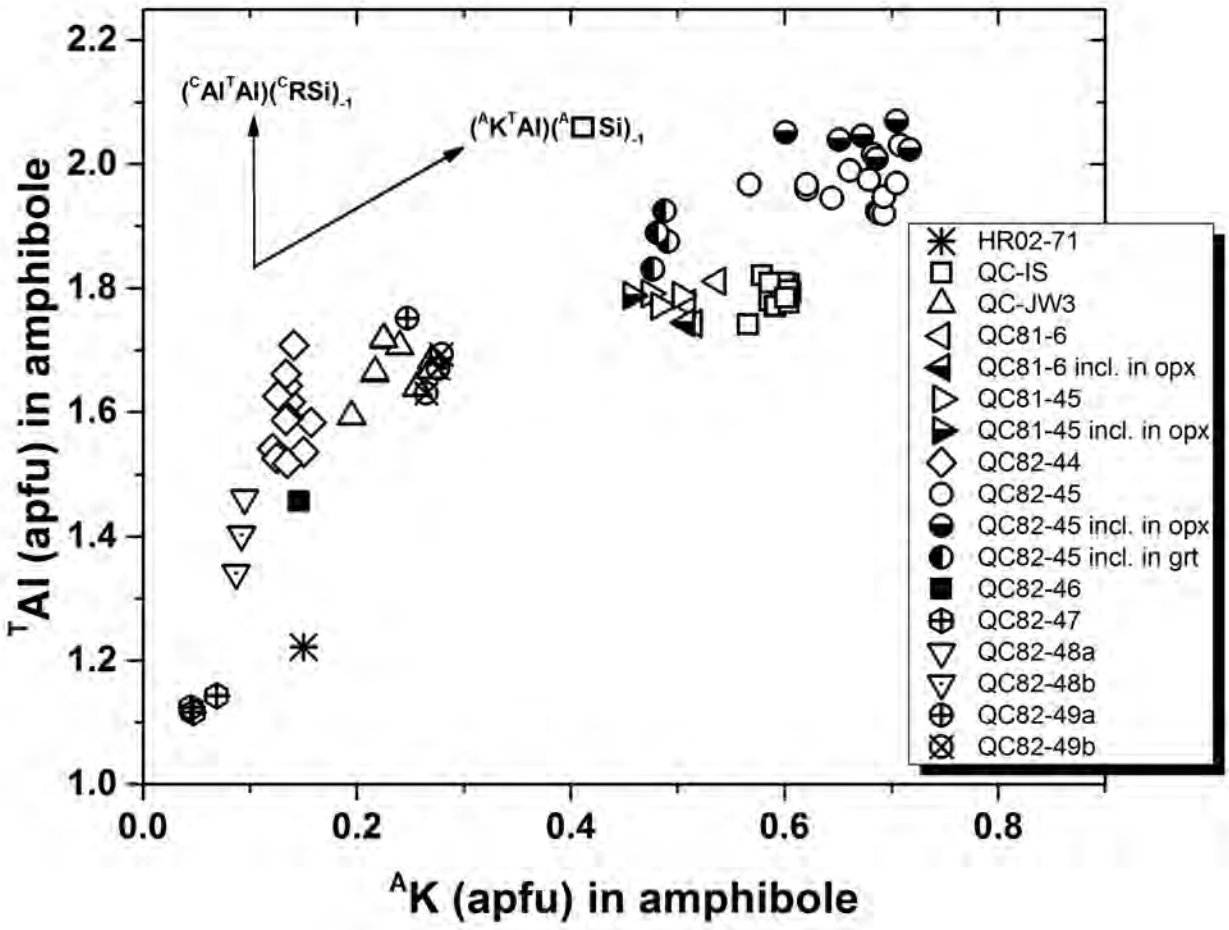

Figure 6A

Always consult and cite the final, published document. See http:/www.minsocam.org or GeoscienceWorld

This is a preprint, the final version is subject to change, of the American Mineralogist (MSA)
Cite as Authors (Year) Title. American Mineralogist, in press.
DOI: http://dx.doi.org/10.2138/am-2018-6143

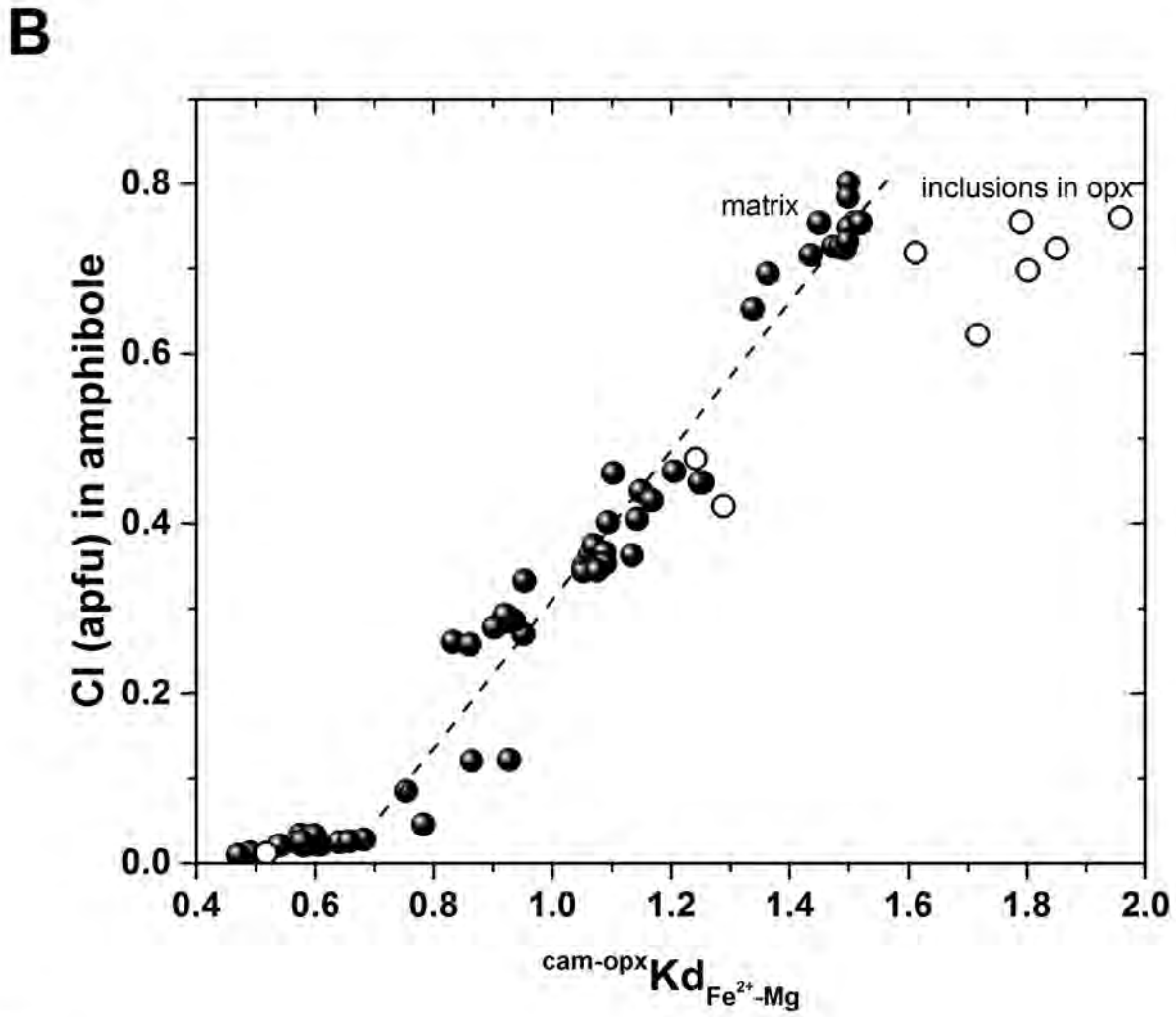

Figure 6B

Always consult and cite the final, published document. See http:/www.minsocam.org or GeoscienceWorld

This is a preprint, the final version is subject to change, of the American Mineralogist (MSA)
Cite as Authors (Year) Title. American Mineralogist, in press.
DOI: http://dx.doi.org/10.2138/am-2018-6143

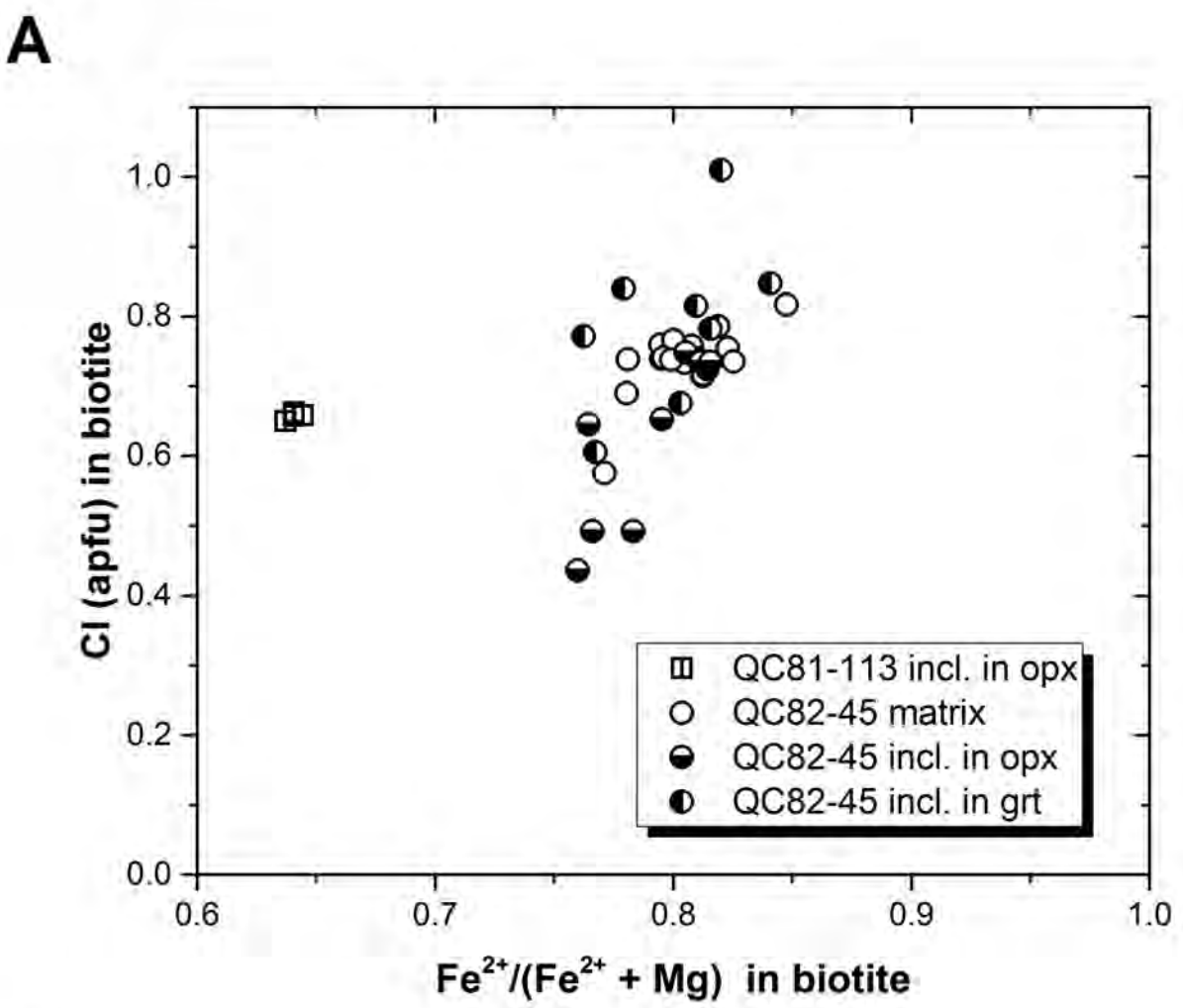

Figure 7A

Always consult and cite the final, published document. See http:/www.minsocam.org or GeoscienceWorld

This is a preprint, the final version is subject to change, of the American Mineralogist (MSA)
Cite as Authors (Year) Title. American Mineralogist, in press.
DOI: http://dx.doi.org/10.2138/am-2018-6143

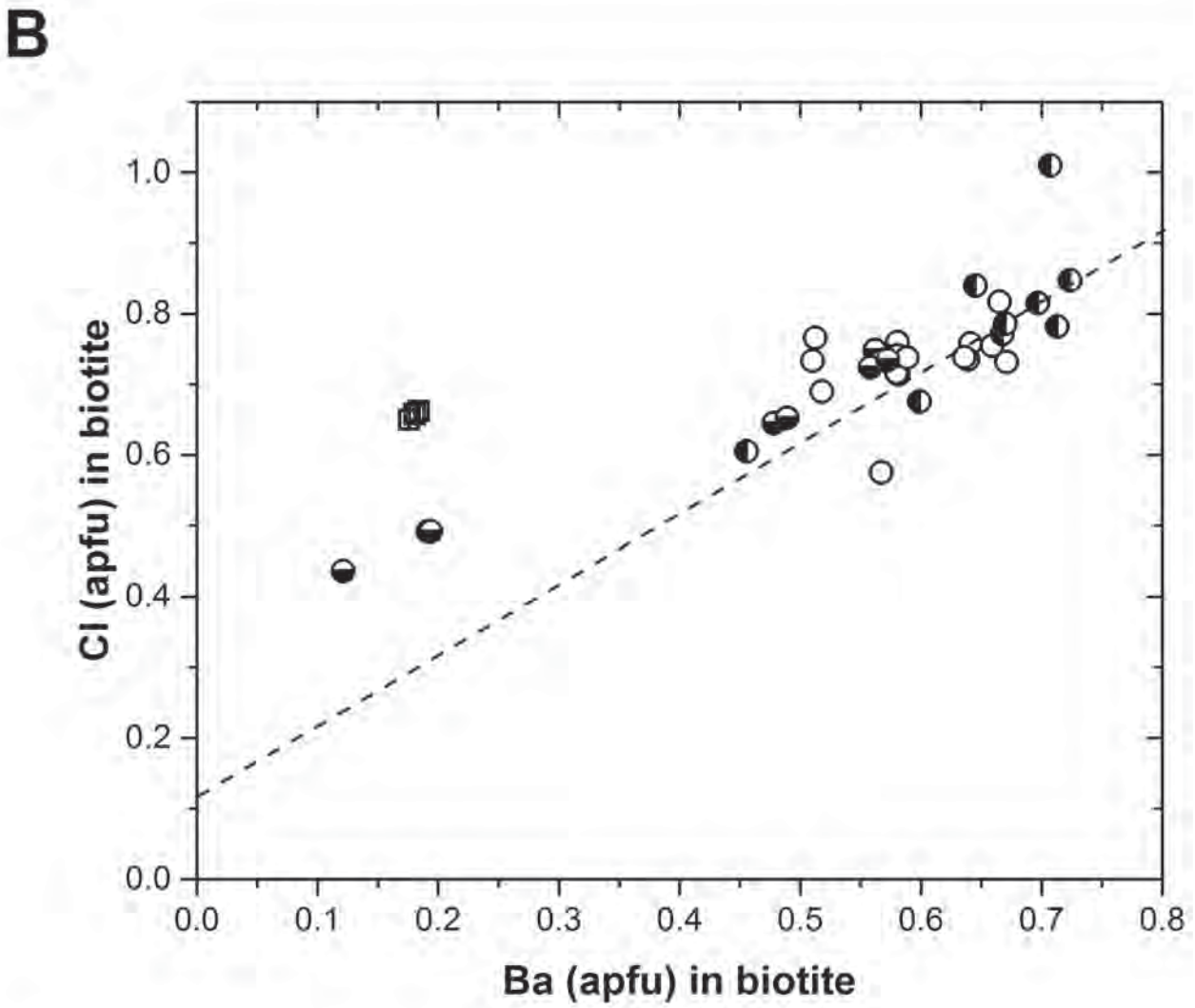

Figure 7B

Always consult and cite the final, published document. See http:/www.minsocam.org or GeoscienceWorld

This is a preprint, the final version is subject to change, of the American Mineralogist (MSA)
Cite as Authors (Year) Title. American Mineralogist, in press.
DOI: http://dx.doi.org/10.2138/am-2018-6143

C

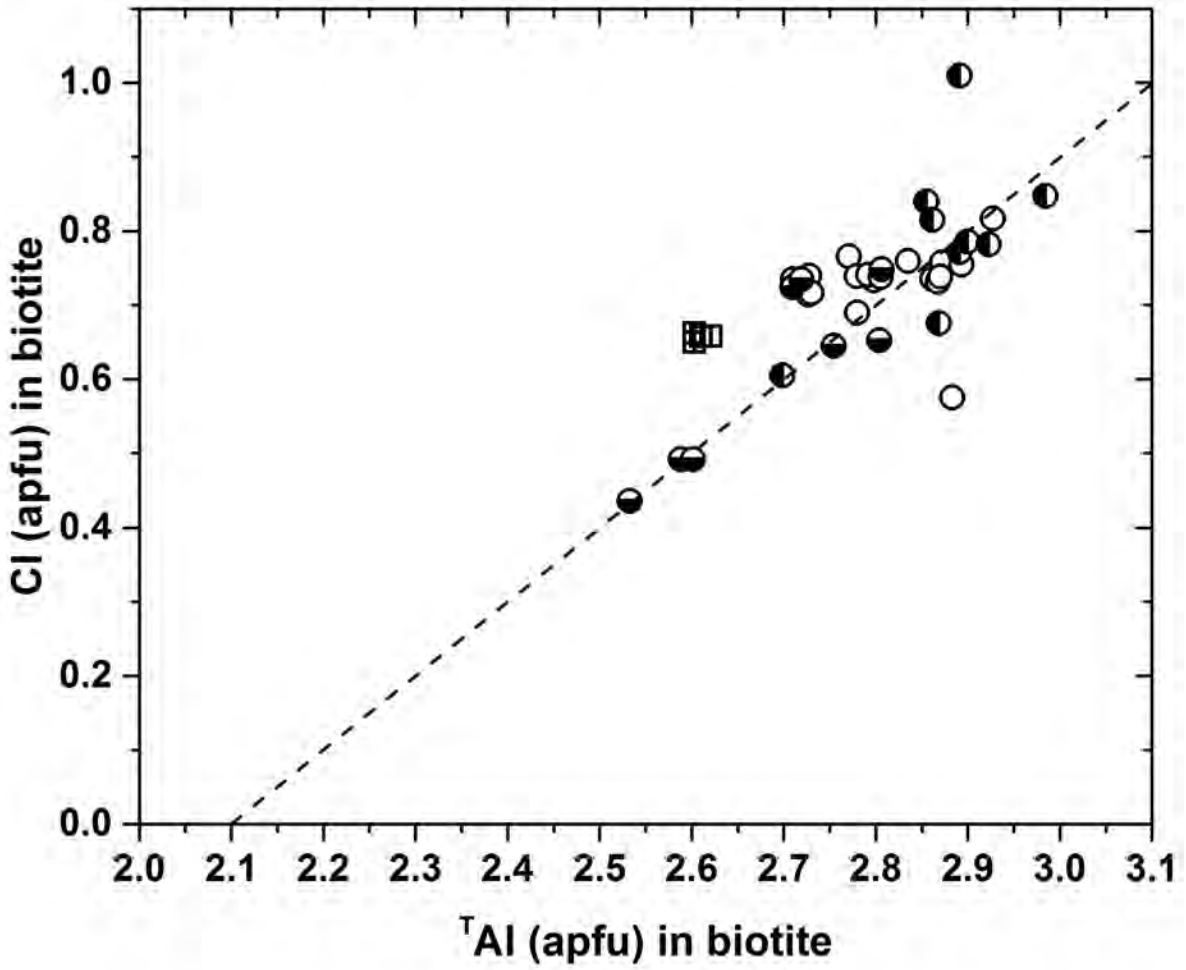

Figure 7C

Always consult and cite the final, published document. See http:/www.minsocam.org or GeoscienceWorld

This is a preprint, the final version is subject to change, of the American Mineralogist (MSA)
Cite as Authors (Year) Title. American Mineralogist, in press.
DOI: http://dx.doi.org/10.2138/am-2018-6143

D

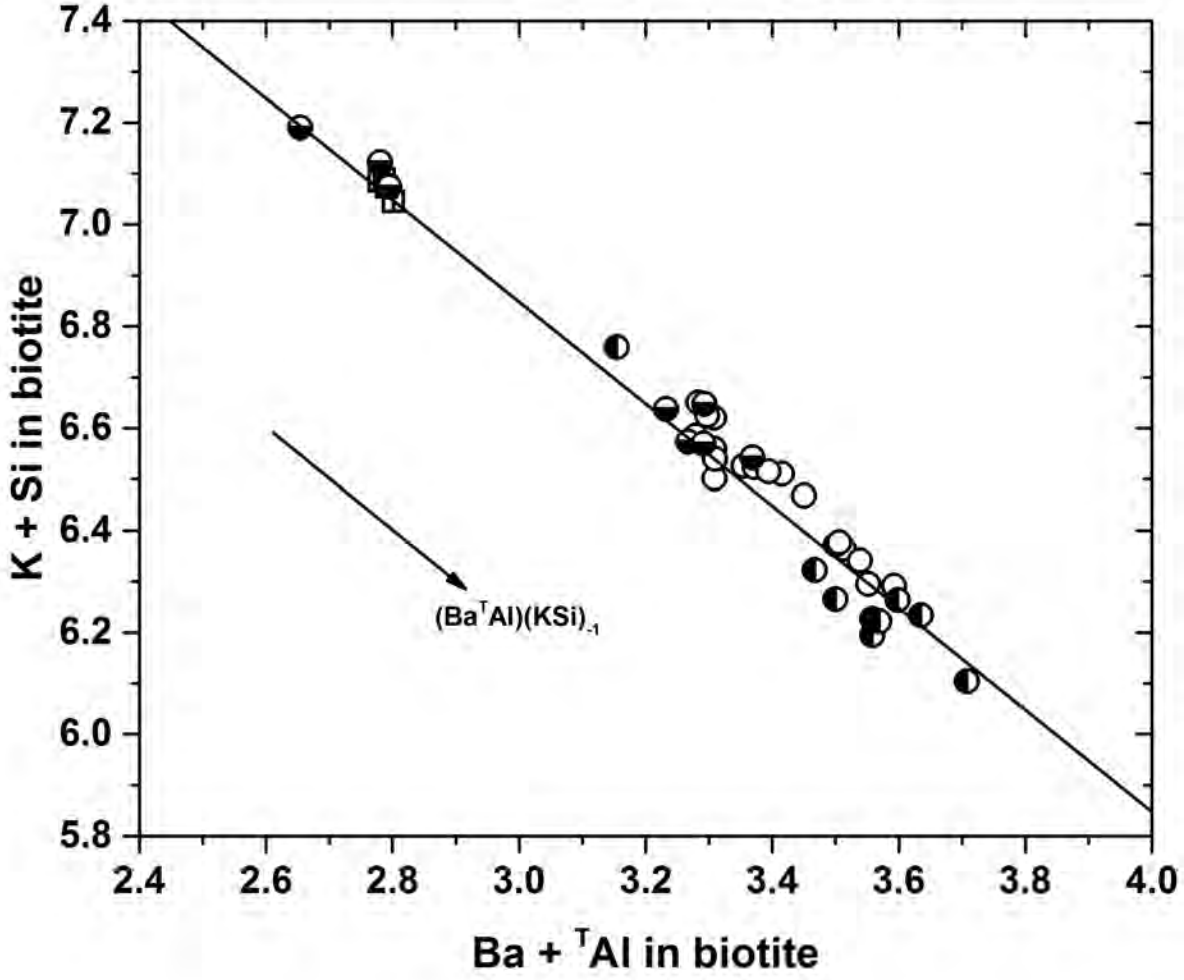

Figure 7D

Always consult and cite the final, published document. See http:/www.minsocam.org or GeoscienceWorld

This is a preprint, the final version is subject to change, of the American Mineralogist (MSA)
Cite as Authors (Year) Title. American Mineralogist, in press.
DOI: http://dx.doi.org/10.2138/am-2018-6143

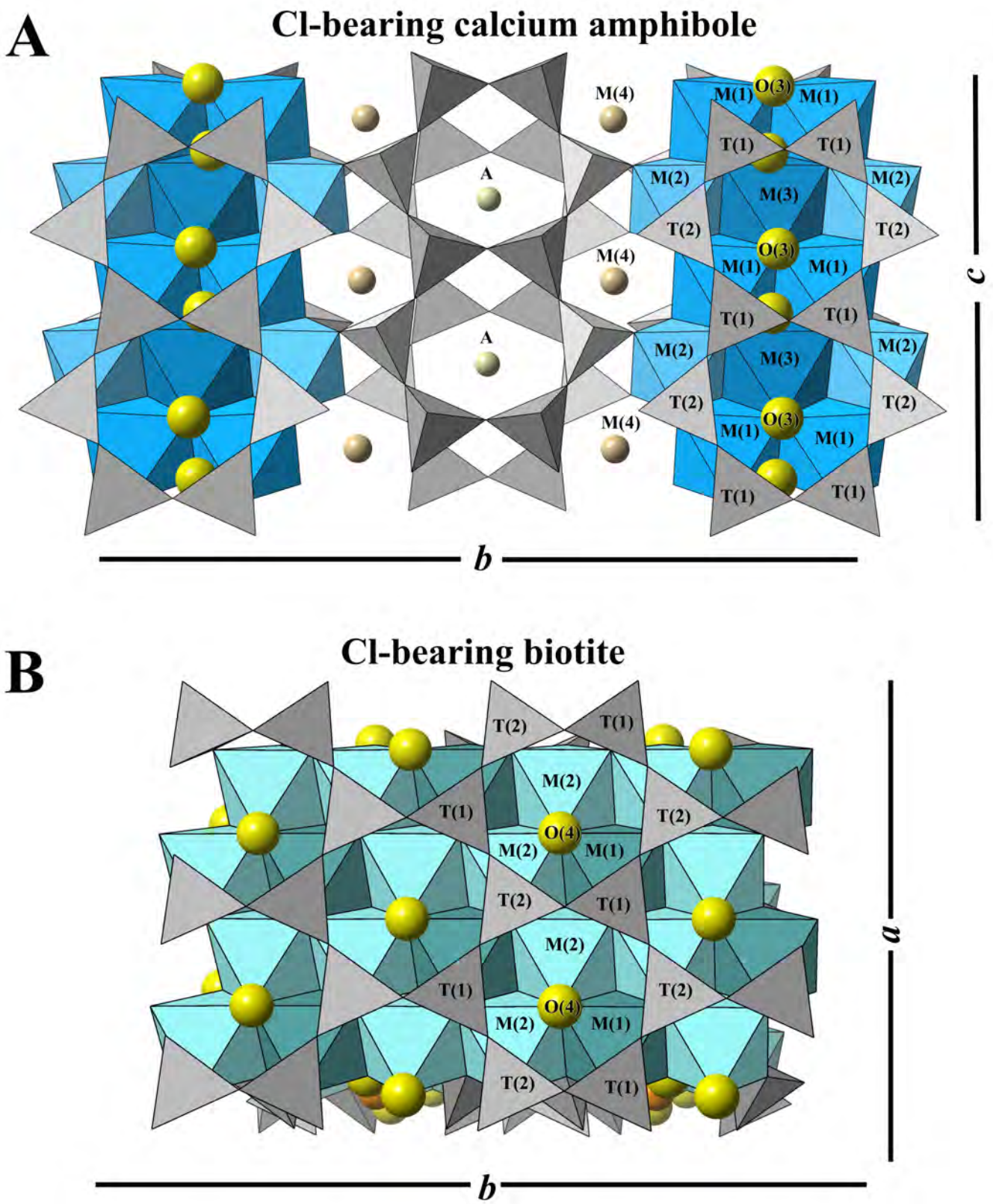

Figure 8

Always consult and cite the final, published document. See http:/www.minsocam.org or GeoscienceWorld

This is a preprint, the final version is subject to change, of the American Mineralogist (MSA)
Cite as Authors (Year) Title. American Mineralogist, in press.
DOI: http://dx.doi.org/10.2138/am-2018-6143

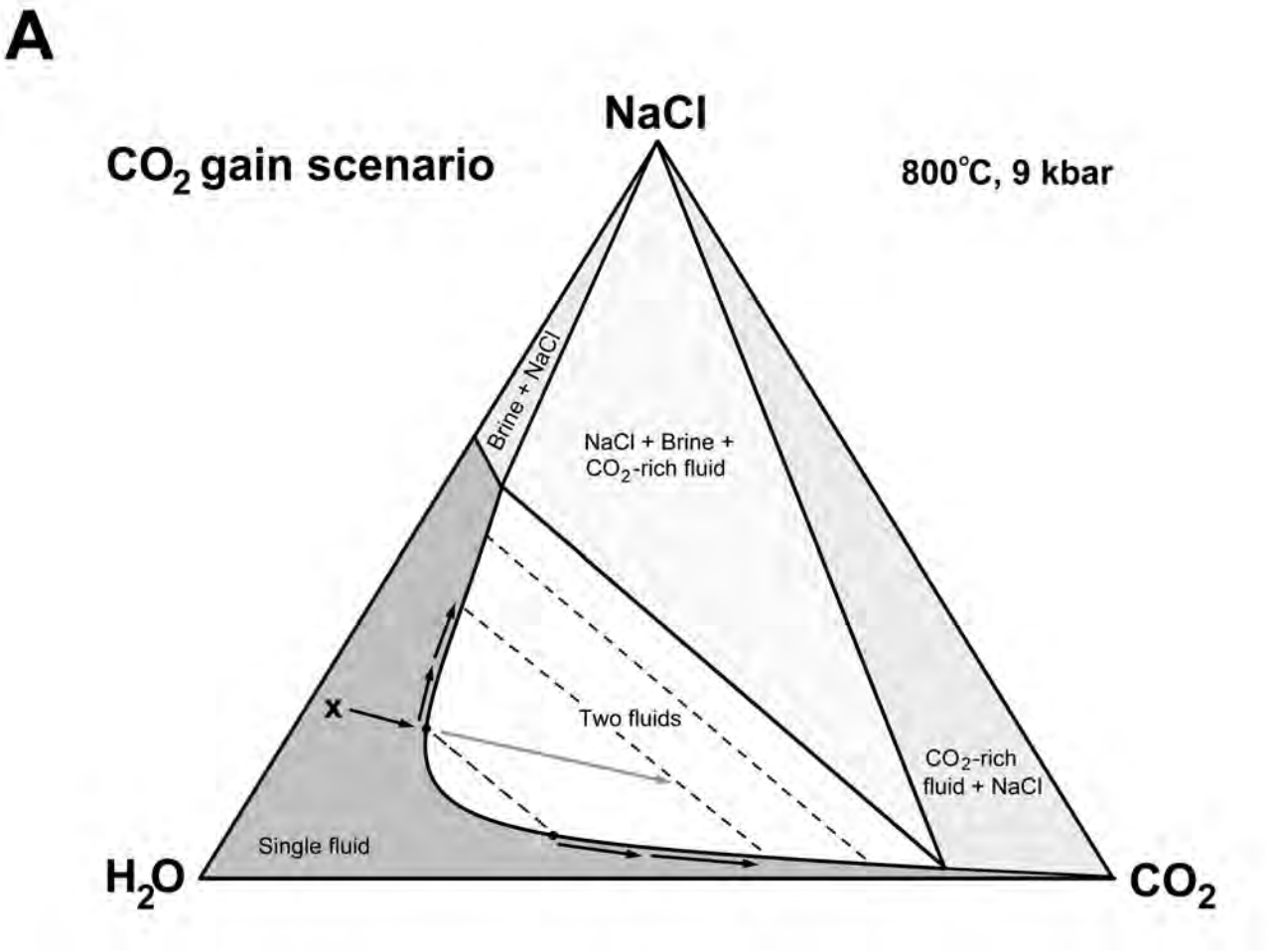

Figure 9A

Always consult and cite the final, published document. See http:/www.minsocam.org or GeoscienceWorld

This is a preprint, the final version is subject to change, of the American Mineralogist (MSA)
Cite as Authors (Year) Title. American Mineralogist, in press.
DOI: http://dx.doi.org/10.2138/am-2018-6143

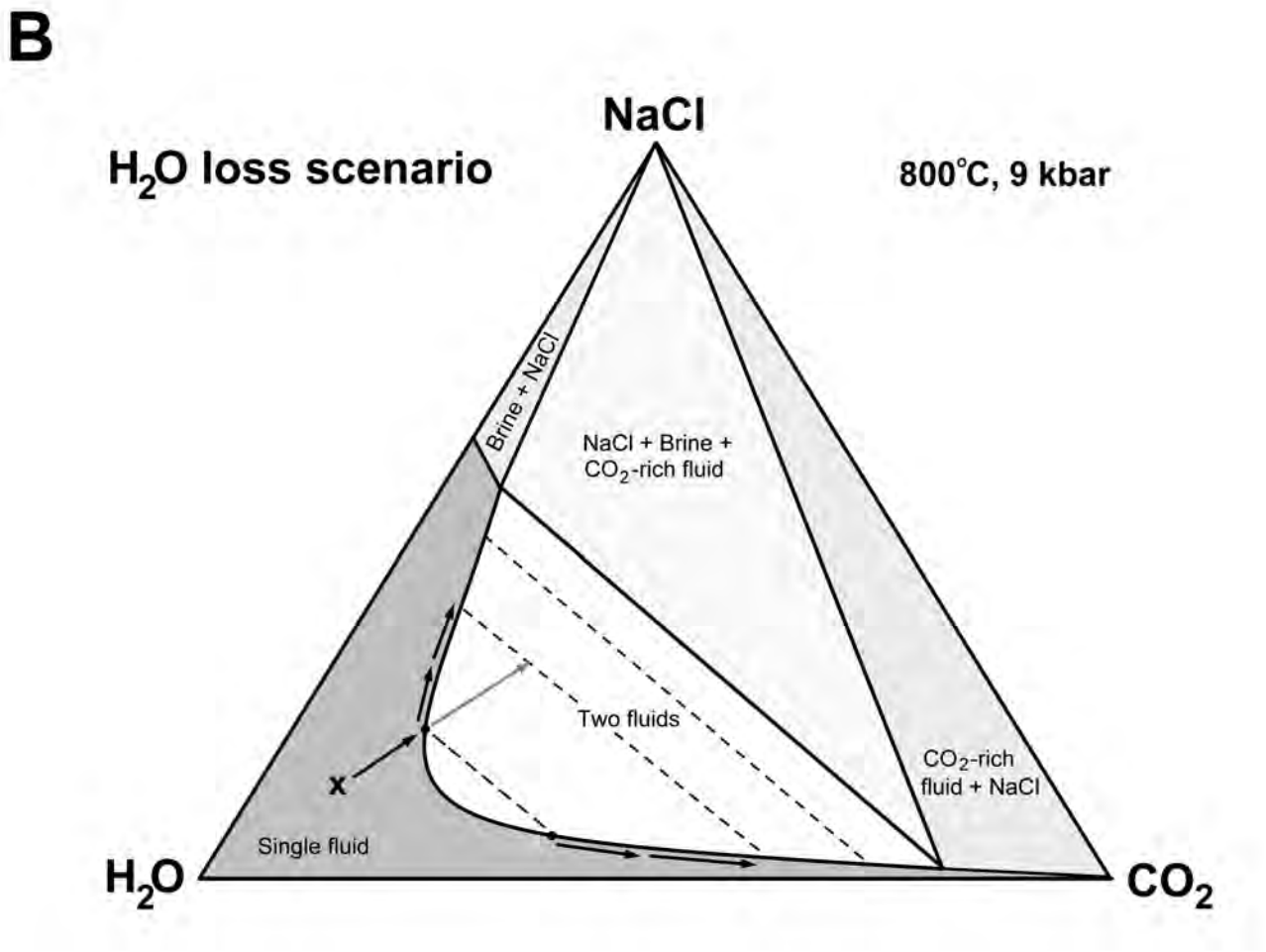

Figure 19B

Always consult and cite the final, published document. See http:/www.minsocam.org or GeoscienceWorld